

Sustainable carbon sources for green laser-induced graphene: A perspective on fundamental principles, applications, and challenges


F SCI


Cite as: Appl. Phys. Rev. **9**, 041305 (2022); <https://doi.org/10.1063/5.0100785>

Submitted: 26 May 2022 • Accepted: 10 October 2022 • Published Online: 10 November 2022

 Pedro I. C. Claro,  Tomás Pinheiro,  Sara L. Silvestre, et al.

COLLECTIONS

 This paper was selected as Featured

 This paper was selected as Scilight



View Online



Export Citation



CrossMark

ARTICLES YOU MAY BE INTERESTED IN

[100 years of Brillouin scattering: Historical and future perspectives](#)



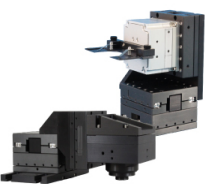
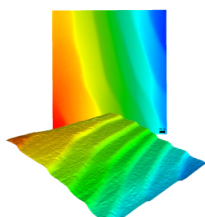
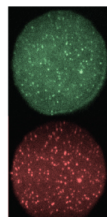
Applied Physics Reviews **9**, 041306 (2022); <https://doi.org/10.1063/5.0095488>

[Advanced thermal sensing techniques for characterizing the physical properties of skin](#)

Applied Physics Reviews **9**, 041307 (2022); <https://doi.org/10.1063/5.0095157>

[Producing graphene sustainably using common organic materials](#)

Scilight **2022**, 461112 (2022); <https://doi.org/10.1063/10.0015151>

 MCL MAD CITY LABS INC. www.madcitylabs.com	<p>Nanopositioning Systems</p> 	<p>Modular Motion Control</p> 	<p>AFM and NSOM Instruments</p> 	<p>Single Molecule Microscopes</p> 
-----------------------------------------------------------------------------------------------------------------------------------------------------------------------------------------	--------------------------------------------------------------------------------------------------------------------	--------------------------------------------------------------------------------------------------------------------	-----------------------------------------------------------------------------------------------------------------------	--------------------------------------------------------------------------------------------------------------------------

Sustainable carbon sources for green laser-induced graphene: A perspective on fundamental principles, applications, and challenges



Cite as: Appl. Phys. Rev. 9, 041305 (2022); doi: 10.1063/5.0100785

Submitted: 26 May 2022 · Accepted: 10 October 2022 ·

Published Online: 10 November 2022



Pedro I. C. Claro,^{1,2,a)} Tomás Pinheiro,² Sara L. Silvestre,² Ana C. Marques,² João Coelho,²
José M. Marconcini,³ Elvira Fortunato,² Luiz H. C. Mattoso,^{3,b)} and Rodrigo Martins^{2,c)}

AFFILIATIONS

¹Graduate Program in Materials Science and Engineering (PPG-CEM), Federal University of São Carlos, São Carlos, São Paulo, 13565-905, Brazil

²IN|CENIMAT, Department of Materials Science, Faculty of Science and Technology, Universidade NOVA de Lisboa and CEMOP/UNINOVA, Campus de Caparica, Caparica 2829-516, Portugal

³Nanotechnology National Laboratory for Agriculture (LNNA), Embrapa Instrumentation, São Carlos, São Paulo, 13560-970, Brazil

^{a)}Author to whom correspondence should be addressed: pedrocunhaclaro@gmail.com

^{b)}Electronic address: luiz.mattoso@embrapa.br

^{c)}Electronic address: rm@uninova.pt

ABSTRACT

Since the discovery of laser-induced graphene (LIG), significant advances have been made to obtain green LIG (gLIG) from abundant, eco-friendly, natural, and organic renewable bio-based carbon sources. Recently, some sustainable and cost-effective electronic devices have been designed with gLIG, resulting in diverse solutions to the environmental impact caused by electronic waste (e-waste). However, there are still several challenges that must be addressed regarding the widespread market implementation of gLIG-based products, from synthesis to practical applications. In this review, we focus on sustainable precursor sources, their conversion mechanisms, physical and chemical properties and applications, along with the challenges related to its implementation, showing the future opportunities and perspectives related to this promising new material. Various systems based on gLIG for energy storage, electrocatalysis, water treatment, and sensors have been reported in the literature. Additionally, gLIG has been proposed for ink formulation or incorporation into polymer matrices, to further expand its use to non-carbon-based substrates or applications for which pristine LIG cannot be directly used. In this way, it is possible to apply gLIG on diverse substrates, aiming at emerging wearable and edible electronics. Thus, this review will bring an overview of gLIG developments, in accordance with the European Green Deal, the United Nations Sustainable Development Goals and the new era of internet-of-things, which demands cost-effective electronic components based on the principles of energy efficiency and sustainable production methods.

© 2022 Author(s). All article content, except where otherwise noted, is licensed under a Creative Commons Attribution (CC BY) license (<http://creativecommons.org/licenses/by/4.0/>). <https://doi.org/10.1063/5.0100785>

TABLE OF CONTENTS

I. INTRODUCTION	2	1. Raman spectroscopy characterization of green LIG	8
II. OVERVIEW ON GREEN LIG FUNDAMENTAL PRINCIPLES	3	2. X-ray photoelectron spectroscopy (XPS) characterization of green LIG	10
A. Conversion mechanism for green LIG	3	3. Electrical conductivity of green LIG	10
1. Laser operational parameters governing the synthesis of green LIG	3	4. Morphological characterization of green LIG	11
2. Aromatic bio-based sources	6	III. TECHNOLOGICAL APPLICATIONS FOR GREEN LIG	11
3. Aliphatic bio-based sources	7	A. Sources of green LIG from raw materials	12
B. Physical, chemical, and conductive properties of green LIG	8	B. Sources of green LIG from processed by-products	15
		1. Lignin	16

2. Paper and nanocellulose	17
C. Other potential bio-based sources	21
IV. OUTLOOK AND CHALLENGES OF ELECTRONIC DEVICES BASED ON GREEN LIG	23

I. INTRODUCTION

Since its discovery in 2004, graphene and similar two-dimensional (2D) nanomaterials have been intensively studied, with some products already commercially available, due to their remarkable set of physical and chemical properties.^{1–6} Graphene is a one-atom-thick sheet of sp²-hybridized carbon atoms, arranged in a honeycomb lattice where each atom shares with its neighbors three in-plane σ -bonds and an out-of-plane π -bond, with an average interatomic distance of 1.42 Å. Due to its unique combination of crystallographic and electronic structures, this material exhibits high surface areas (2630 m²·g⁻¹), carrier mobility ($\sim 250\,000$ cm²·V⁻¹·s⁻¹), thermal conductivity (around 2000–4000 W·m⁻¹·K⁻¹), and transmittance [visible light and near-infrared (IR) absorption $\sim 2\%$ – 3%] along with excellent mechanical properties (Young's modulus: 1×10^{12} Pa), good chemical stability, and biocompatibility.^{7–9} Owing to its distinctive properties, graphene has proven to be broadly applicable in several areas, such as energy storage, sensors, electronics, catalysis, environmental remediation, and biotechnology.^{10–17} Moreover, graphene can be engineered into three-dimensional (3D) porous structures to render higher surface areas while maintaining its high mobility and mechanical stability.^{18–21}

However, despite intensive research efforts, chemical-free, low temperature, and cost-effective processing of high-quality graphene remains a massive challenge.⁸ Conventionally, graphene can be produced with different physical and chemical-based techniques. This includes mechanical exfoliation (scotch tape) of graphite, chemical vapor deposition onto metallic substrates from gaseous hydrocarbon precursors, thermal decomposition, and reduction of graphene oxide (GO).^{9,22} Despite tremendous advances, these methods require either high processing temperatures, multi-step synthesis routes, and/or the use of expensive precursors, which significantly limits the scale-up of the current production methods, restricting their widespread commercial potential. Therefore, straightforward production methods that allow for simple, cost-effective, and scalable graphene-based material's production and patterning are absolutely needed.^{23,24}

In this context, laser-assisted processing techniques have emerged as powerful tools for a multitude of applications, from materials processing to device manufacturing.²⁵ Specifically, laser-direct writing (LDW) is a mask-less, catalyst free, nontoxic, controllable, and non-contact approach method, allowing flexible, rapid, direct, and efficient processing of complex structures for laser macro-, micro-, and nano-subtractive manufacturing.⁸ In fact, LDW was reported in a few works for the conversion of graphene oxide (GO) to graphene for the development of functional components.^{26,27} In 2014, James Tour's research group from Rice University reported a method to induce 3D porous graphene by direct conversion of polymeric substrates using LDW, which was denominated as laser-induced graphene (LIG).²⁸ As the group stated in a subsequent publication, the discovery of LIG was a fluke: "This was a serendipitous discovery when J. Lin of our group was attempting to lase GO dispersed upon a PI film. The laser missed the GO target and the PI was lased, becoming black. Upon checking the

Raman spectrum, Lin noticed that the PI-bound black material was graphene."²⁵ This accidental conversion of commercially available polymers to LIG, such as polyimide (PI), was achieved by using a common CO₂ laser system—with a wavelength of 10.6 μm —often found in workshops for cutting and engraving purposes.²⁸ The chemical structure of PI is particularly suitable for the generation of LIG, owing to the presence of aromatic sp² carbons that are more prone to form the hexagonal graphene structure than other precursors, which just generate amorphous carbon. Additionally, PI is also known for its high thermal resistance, therefore withstanding the thermal gradients verified during the laser engraving process.⁹

Recent efforts have been made to produce LIG from other carbon-based substrates—LIG can now be obtained from a variety of materials, ranging from thermoplastic polymers, phenolic resins, bio-polymers like lignin and even textiles, cellulose, wood, cork, or even food (e.g., potato skins, bread, and coconut shells), and its versatility and potential has been demonstrated in several applications. Of special interest has been the recent rise in the synthesis of LIG from natural, bio-based substrates and its use in several electronic applications, as showed in Fig. 1.^{1,9,28–48}

This review aims at providing a comprehensive overview focused on the synthesis, properties, and application of LIG synthesized from natural, organic bio-based precursors, that present improvements in terms of their accessibility and sustainability, termed green LIG (gLIG). Such bio-based substrates include easily accessible and abundant raw materials, such as wood, leaves, cork, husks, coal, and food. More recently, the versatility of such materials, in terms of their chemical compositions and the possibility to process them into highly valuable goods, has sparked a steep growth of the application of their by-products for laser irradiation and gLIG synthesis. These include lignin, cellulose substrates, such as paper and nanocellulose, and other formulations, where the initial chemical composition and mechanical properties of the precursor substrates can be tailored for optimal irradiation and graphitization outcomes.^{32,49–51} Laser irradiation principles, guiding the graphitization processes leading to the synthesis of gLIG, are thoroughly discussed in this review. First, laser operational parameters modeling the photochemical and/or photothermal effects responsible for substrate conversion are discussed, in terms of the ability to manipulate the graphitization processes. The chemical specificity of different natural bio-based precursor substrates is outlined, in terms of their aromatic or aliphatic natures, and how these different chemical structures lead to different conversion pathways and to gLIG synthesis. The properties and characterization of several gLIG surfaces reported in the literature are systematized and exhibited in a comprehensive way. Therefore, it is established mechanistic principles that can guide future characterization of gLIG synthesized from different bio-based precursors, using distinct laser systems. With strong understanding of these processes and graphitization outcomes, the development of emerging electronic devices based on gLIG approaches is also discussed. Finally, we provide an overview of gLIG societal impact and its importance as a material obtained from subtractive manufacturing toward zero electronic waste (e-waste).^{18,52} This review distinguishes itself by focusing only on gLIG, while detailing the challenges and perspectives of its application based on current environmental, and socioeconomic agreements and goals.

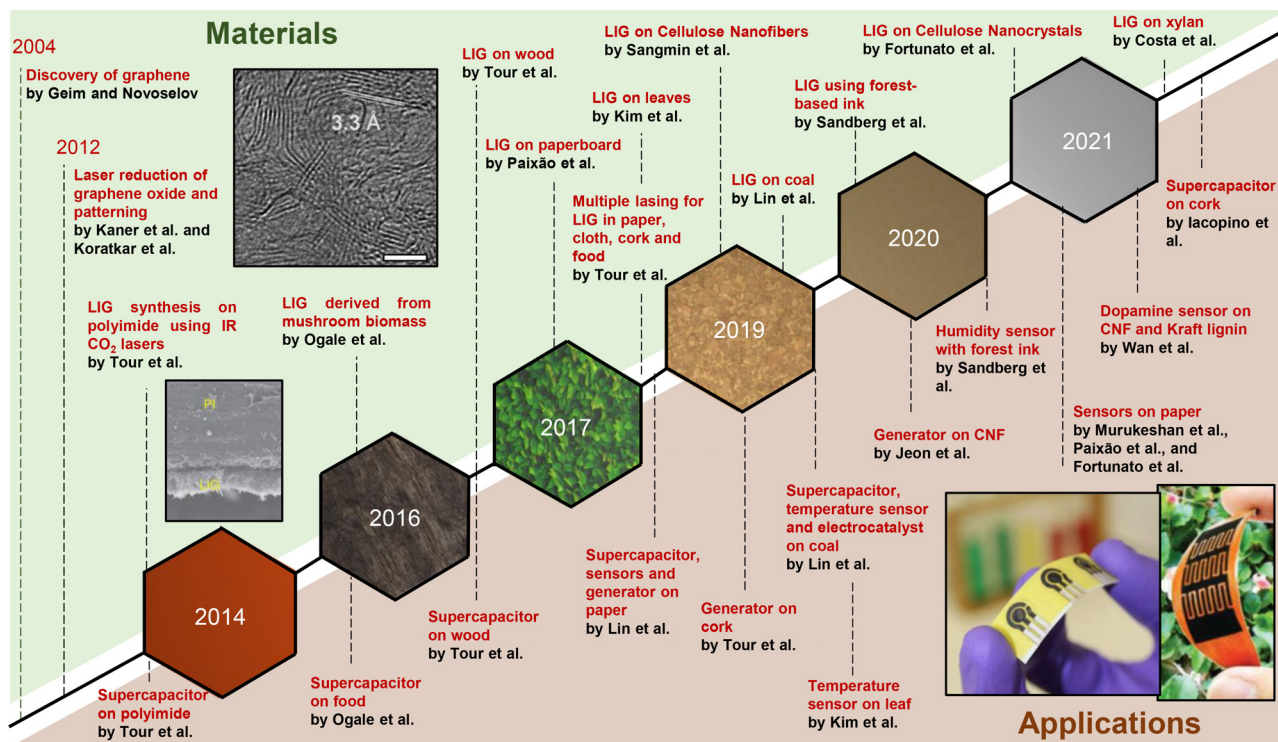


FIG. 1. Main landmarks of green LIG based on novel precursor materials and their applications with green LIG. TEM image reproduced with permission from Ye *et al.*, *Adv. Mater.* **29**, 1702211 (2017). Copyright 2017 John Wiley and Sons.⁴³ SEM image reprinted by permission from Lin *et al.*, *Nat. Commun.* **5**, 5714 (2014). Copyright 2014 Springer Nature.²⁸ Supercapacitor illustrative image reproduced with permission from Le *et al.*, *Adv. Funct. Mater.* **32**, 2107768 (2022). Copyright 2022 John Wiley and Sons.⁴¹

II. OVERVIEW ON GREEN LIG FUNDAMENTAL PRINCIPLES

A. Conversion mechanism for green LIG

Green LIG is an emerging and trendy carbon material obtained by LDW of several bio-based carbon sources and substrates, such as wood, leaves, cork, husks, and cellulose [Fig. 2(a)].⁴² The graphitization occurs by photothermal and/or photochemical effects, upon which surface carbon atoms are converted from sp^3 to sp^2 dominated configurations, with some differences in chemical reactions depending on the aromatic or aliphatic nature and composition of the substrates. Furthermore, different laser systems and their operational parameters influence this conversion, namely, in terms of bond breaking, their rearrangement and the efficiency of these processes in the synthesis of graphitic carbon forms that characterize gLIG. In this section, laser radiation induced conversion processes and their manipulation are addressed. Laser source wavelength characteristics, aspects related to laser fluence, and the chemical characteristics of the precursor materials are discussed.

1. Laser operational parameters governing the synthesis of green LIG

Laser photodegradation of polymers of different origins has been a well-studied phenomenon, pertaining to different outcomes, including bond degradation for the synthesis of refined chemical species, conversion processes for materials' synthesis or complete ablation of

the material, such as in photolithography.^{53,54} These laser-induced photophysical processes have been distinguished by two complementary models, namely, photochemical and photothermal effects over the polymer volume. Photochemical effects are related to electronic excitation by incident photons with sufficient energy, which can lead to bond isomerization, forming, and breaking.⁵⁵ Photothermal effects occur due to localized heat ramps, caused by the incident laser beam, leading to bond cleavage, rearrangement of bonds, and in cases of excessive exposure, to complete ablation of the irradiated material. While photochemical bond breaking is more dependent on the wavelength of the laser photons and how they interact with specific bonds within the chemical structure of the precursor material, photothermal effects depend more on the set of operational parameters, such as laser power, pulse repetition rate, and pulse length, that control the optical fluence and the resulting imposed temperatures.⁵⁶

In the context of graphitization processes for gLIG synthesis, there may be the combination of photochemical and thermochemical mechanisms, depending on the laser source wavelength and irradiation regimens, that leads to bond breaking and rearrangement within natural organic polymers. Depending on the chemical composition of the irradiated natural organic substrate and the selected laser source, specific bonds are more prone to be degraded and cleaved by photochemical processes within the natural substrates, to cause depolymerization of the polymeric structure and cleave undesired carbon-oxygen bonds.^{57–59} Although the role of photochemical processes in gLIG synthesis is still unclear, most authors report that different laser

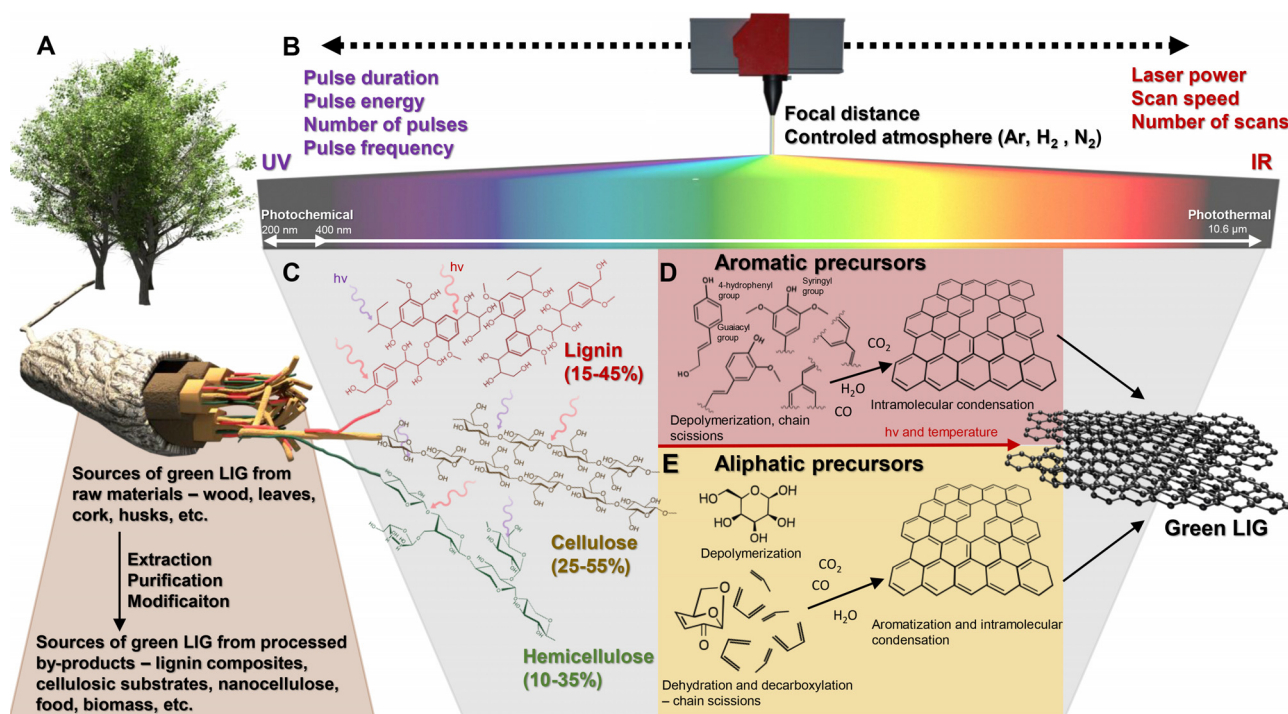


FIG. 2. Schematic illustration of the conversion mechanism for green LIG. (a) Sources of green LIG from raw materials and processed by-products obtained from these natural sources. (b) Laser parameters employed in the bio-based carbon conversion to green LIG. (c) Macromolecule chemical structure of lignocellulose biopolymers, its range composition on natural sources, and the local laser irradiation interaction in macromolecules. (d) and (e) Aromatic and aliphatic chemical mechanism conversion to green LIG, respectively.

wavelengths have different dynamics in this process, due to the contribution of photochemical phenomenon.⁶⁰ Thus, the onset of carbonization and graphitization has been mostly attributed to photothermal processes that become dominant. These effects impose temperature gradients that not only complement the breaking of covalent bonds but simultaneously promote fast reorganization of atom vacancies and improve carbon atom layout, leading to graphitization. The incident laser radiation must induce phonons in the material, with vibrational energies that decompose weaker bonds and components, leading to microablation and release of volatiles.⁶¹ These become ionized and form a plasma discharge, characterized by bright flashes over the irradiated substrate. This plasma plume serves as a shield for further penetration of the laser beam and generates very high localized temperatures, upon which carbonization and graphitization occur, through the rearrangement of cleaved carbon bonds by aromatization and condensation processes, leading to the synthesis of sp^2 carbon-rich lattice domains that constitute gLIG.

Laser sources ranging from ultraviolet (UV) to IR wavelengths have been employed being carbon dioxide (CO_2) lasers with $10.6 \mu m$ photon wavelength the most commonly used for these purposes.⁶² Lasers that emit UV radiation (200–400 nm wavelength) have the highest photon energy, above the dissociation energies of various substrates chemical bonds, that can lead to the necessary cleavage before their rearrangement into gLIG chemical structures.⁶³ For instance, the photodegradation of cellulose structures when exposed to photon energies above $3.6 eV$ ($\lambda < 340 nm$) induces direct photolysis or

photo-oxidative degradation of some chemical bonds.⁶⁴ Thus, excimer and UV lasers that emit high-energy photons with uniform spatial distribution, can promote photochemical reactions by directly breaking the chemical bonds of carbon precursors. Because of that, radiation emitted in or near the UV region has lower penetrating power in some bio-based carbon sources, carbonizing the top of the sample without significantly heating the sample. However, both photothermal and photochemical bond breaking occur when using these lower wavelength laser sources, depending on the imposed fluence. For lower fluences, there is a dominance of photochemical reactions, while the contribution of photothermal effects rise for higher fluences, where each unit of area is exposed for prolonged periods of time.⁶⁵ On the other hand, CO_2 lasers emit IR radiation, with lower photon energy, which is less able to directly break covalent bonds. However, they cause significant heating of the substrates, inducing thermochemical reactions resulting in the breaking of covalent bonds. The same was observed for solid-state lasers (e.g., Nd:YAG lasers) and others visible light diode lasers (LightScribe) that emit radiation near to IR.^{8,66} It is important to note that these types of lasers present some differences in relation to CO_2 lasers, such as fast galvo scanning systems, thus presenting a high potential for large scale gLIG production. Thus, the selection of an appropriate laser source is important, taking into account several aspects. These include the substrate light absorption that promotes efficient photon induced heating at appropriate fluence regimens, while also considering aspects regarding geometrical resolution, related to laser spot size. Typical CO_2 lasers present spot sizes in

hundreds of μm ,²⁸ while visible and UV lasers can achieve much higher spatial resolution.⁶²

Complementing the effects of the laser source wavelength regarding degradation of chemical structures within gLIG precursors, meticulous control of laser operational parameters is paramount to tailor the photothermal effects responsible for graphitization of the substrate. Depending on the laser system, different parameters have been manipulated, to control the laser fluence over the substrate. Fluence is the optical energy delivered to the substrate by unit of area, measured in J cm^{-2} , and influences the outcomes of the irradiation process, since it dictates the resulting imposed temperatures and the resulting energy units for carbonization and graphitization. Operational variables, including laser source power, laser beam scan speed, pulse density, irradiation focal plane, and the number of irradiation cycles, define this fluence and are discussed below [Fig. 2(b)].

Laser source power is the key parameter in the control of input energy over the substrate. Depending on the selected laser system and its maximum power output, tuning of the irradiation power provides a means of controlling the energy that is delivered to the surface of the substrate and the resulting temperature ramp that promotes bond cleavage and subsequent reorganization, without excessive degradation and ablation. As some authors suggested, increasing the lasing power ultimately leads to increased localized temperatures in the substrate that helps promote the necessary breaking of bonds more efficiently, leading to less oxygen content in the synthesized chars or graphitic structures.⁶⁷ Some authors even suggest that these processes happen at specific temperature, as is the case when using nanocellulose structures.⁶⁸ The selection of optimized laser power and its influence over the graphitization are not an independent variable and are usually associated with its distribution for the selected irradiation regimen. Predominantly, raster processes have been selected to synthesize and pattern gLIG simultaneously. The scanning speed of the raster processes has been a key parameter in gLIG synthesis since it influences the spread of irradiation energy for both continuous wave (CW) or pulsed irradiation regimens and selected pulse profile. For lower scanning speeds, the area exposed to each individual pulse is smaller, increasing the laser fluence, usually leading to greater degrees of graphitization until a certain threshold, above which, laser fluence causes excessive ablation of the precursor material. In opposition, higher scanning speed causes a larger spread of laser beam energy, leading to a decrease in energy exposure for each unit of area. Usually, authors have resorted to establishing, which power and scanning speed pairs are able to synthesize gLIG, in opposition to outcomes related to inefficient carbonization or excessive degradation and ablation of patterns. Usually, power values that cause degradation and ablation must be offset with higher scanning speeds, while power values unable to cause carbonization and graphitization must be complemented with lower scanning speeds, thus achieving conducive fluence regimens for efficient yield.

Complementing the effects of laser power and scanning speed, pulse energy distribution manipulation has been studied. Pulse density over the irradiated area has been manipulated using various laser systems, from UV to IR CO_2 lasers, allowing the tuning of repetition rate. Parameters, such as number of pulses per inch (PPI) or switching frequencies on pulsed laser systems, enable a versatile control of the fabrication parameters. By employing regimens with higher pulse frequency, irradiation profiles closer to continuous wave irradiation

can be reached, easily increasing the laser fluence for higher pulse densities. Another important aspect of pulse density manipulation is the ability to create superposition patterns in laser beam pulse profiles. These are known to increase the graphitization potential,⁶⁹ which is also applicable in several bio-based precursors. In addition to pulse repetition rate, another means of manipulating the pulse profile has been by defocusing of the laser beam, placing the precursor substrate over different laser beam focal planes. This defocusing method takes into consideration the laser beam profiles caused by the optical systems that leads to different beam spot sizes at different focal planes. Upon a defocused irradiation process, larger spot sizes create superposition patterns between subsequent laser pulses, causing the same irradiated area to be multiply lased using a single raster cycle. Thus, carbonization occurs at the substrate for the first pulse, ensued by overlaying irradiation in the subsequent pulse that can be induced the desired graphitization. This leads to increased conversion efficiency within a single rastered line, but also between successive lines within the rastered gLIG pattern, increasing the conversion continuity over the engraved geometry.⁴² Similar increases in graphitization potential and efficiency have also been achieved by employing multiple lasing scans for conversion, mainly in cellulosic precursor substrates.^{32,42} However, careful manipulation of these operational parameters has allowed for single scan irradiation conversion in such substrates, by tuning the input power and its distribution, to create the superposition pulse patterns that mimic the effects of multiple patterning cycles.⁴⁷ Other fabrication parameters intrinsic to each individual type of laser system can also be taken into consideration when modeling gLIG synthesis, including pulse duration, beam profile, its quality, and polarization. In this regard, pulse duration has been a key parameter to achieve more desirable outcomes when synthesizing gLIG from several bio-based sources. Namely, by employing several strategies using ultrashort-pulsed lasers, most prominently, femtosecond (FS) lasers. Combined with photon energy, ultrashort pulse durations, and extremely high peak intensities provided an efficient graphitization of green materials, including wood, leaves and nanocellulose.^{38,41,70} High-resolution patterning ($<50 \mu\text{m}$) under ambient conditions could be achieved, without the need for inert atmospheres or additional chemical treatments. This is because tuned repetition rates, in the kHz frequency range, paired with small pulse duration, allows for a greater control of generated thermal fields and their dissipation. For optimized conditions authors can control these variables to achieve thermal field overlapping and thermal accumulation that increases temperatures that are able to cause graphitization and assist in other processes, such as exfoliation.⁴⁵ This greater control allows for this graphitization to happen in an ambient atmosphere, converting all lignocellulosic precursors without their complete ablation, observed for CO_2 laser irradiation of wood in ambient atmospheres.³⁰

As such, the irradiation atmosphere has appeared as a very important consideration depending on the laser systems and irradiation scheme. In the literature, the effects of the ambient atmosphere and controlled atmospheres with nitrogen (N_2), argon (Ar), and hydrogen (H_2) gas on the reduction of the precursor and removal of undesired carbon-oxygen bonds are reported, impacting the quality of conversion in correlation with laser parameters and source.^{71,72} Atmosphere composition is important to control the degree of graphitization of green materials, preventing its burning, which is directly correlated with the thermal stability provided by the aromatic or

aliphatic chemical structure of the bio-based sources. Furthermore, inert atmospheres provide the higher reducing capability, promoting a more efficient substitution of oxygen moieties, resulting in more stable surfaces. On the other hand, the presence of oxygen in the air can cause higher combustion and oxidation, causing higher volatile formation and porosity.⁴³ This has been important for unmodified wood conversion, where inert atmospheres are a requirement for gLIG synthesis when employing CO₂ lasers. In fact, irradiation in the air causes the combustion of all wood components by oxygen, leading to its ablation instead of graphitization.

Considering the bio-based carbon source, laser operational parameters and atmosphere control, graphitization processes can be tailored to achieve optimal chemical and conductive properties. In addition to the fabrication variables governing these processes, understanding the influence of chemical composition within natural precursor materials is of extreme importance, since they lead to distinct chemical pathways for gLIG formation, as discussed for aromatic and aliphatic green precursors.

2. Aromatic bio-based sources

Lignocellulosic materials found in many used and potential gLIG precursor substrates are the most abundant renewable sources of aromatic chemical structures.⁷³ This is because of the high lignin content of the natural materials, with up to 30% content depending on the biomass source. Lignin contains in its structure an abundance of benzene rings covalently bound to other functional groups, resulting in an amorphous branched aromatic polymer, constituted by three different aromatic ring substitution patterns, namely, p-hydroxyphenyl, guaiacyl, and syringyl monomers [Fig. 2(c)].⁶⁵ When using bio-based gLIG sources containing this aromatic macromolecule, such as wood or even engineered films composed of extracted lignin, the conversion processes and reactions into graphenic structures are based on the breaking of C–C, C–O, and C–H bonds both within and outside the aromatic structures. The reorganization into char-like or graphitic structures occurs afterward, depending on the degree of pyrolytic activity set by the laser irradiation parameters. These principles are analogous to the ones established for PI conversion into LIG, since both these precursors are rich in native aromatic structures. However, each has specificities related to the differences in their chemical structure and the distribution of aromatic moieties over the molecular structure.⁷⁴

When considering the photochemical degradation processes that can occur during the laser irradiation process, specific linkages within the polymeric structures of lignin and their interaction with the incident photons must be considered. Several studies have reported the analysis of UV photodegradation of lignin in wood and kraft pulp, showing that α and β glycosidic bonds are more prone to cleavage, while carbon bonds connecting aromatic structures have resistance to UV irradiation.⁵⁷ This shows that the aromatic backbone of lignin and its connection is usually maintained, allowing for their subsequent reorganization and polymerization into graphene structures. Similar processes have been achieved using IR laser irradiation, by tuning the wavelength to specific vibrational modes of linkages within lignin, leading to depolymerization.⁵⁸ However, photochemical processes alone are not capable to induce graphitization. For the synthesis of more aromatic dense chemical structures leading to gLIG, pyrolytic

processes are needed, in order to further break undesired chemical structures and promote an efficient reorganization. In most pyrolytic reactions of lignin, based on its exposure to varying temperatures and pressures, its decomposition is also based on depolymerization, by breaking of different ether linkages (C–O–C) or condensed C–C bonds, leading to the formation of volatiles and solid carbonized materials identified as chars.⁷⁵ In these cases, the increase in pyrolysis temperature leads to further degradation of chars and lignin monomers, to synthesize highly valuable, refined aromatic chemicals such as phenol or benzene, among others.^{73,75,76} For some conditions, such as in fast pyrolysis, these precursors can be used as precursors for condensation, leading to the synthesis of polycyclic aromatic hydrocarbons (PAHs), with higher density of aromatic structures.⁷⁷

These pyrolysis principles serve as a model to understand the laser irradiation conversion process of gLIG from aromatic-rich lignin. For gLIG synthesis, lignin is exposed to much higher temperatures for much shorter time frames, leading to the occurrence of very fast, similar pyrolytic processes, that can be modeled in two distinct steps: (i) photochemical promoted bond cleavage and laser promoted vibration of atomic networks, resulting in high localized heating of the material, leading to depolymerization, decarboxylation and dehydration, by the cleavage of C–O–C, C–O, C–C, and C–H bonds and subsequent recombination of oxygen, hydrogen, and some carbon into volatiles; (ii) temperature-promoted rearrangement of aromatic compounds and other carbon chemical structures to form condensed graphitic structures dominated by sp² hybridized carbon [Fig. 2(d)]. In terms of the rearrangement of aromatic structures into sp² dominated lattices, reactions governing these phenomena are based on ring closures that define the graphitization process. Although there are several chemical processes for ring closure and stitching for the synthesis of graphene nanostructures from PAHs,⁷⁸ gLIG synthesis ensuing graphitization is promoted by the very fast pyrolysis caused by the laser, that induces structural changes into more thermally stable graphene lattices and their 3D stacked form.

During laser irradiation, both these sub-processes of removal of oxygen functional groups and direct conversion from sp³ to sp² dominated structures coexist and are manipulated by laser operation parameters dictating the level of laser exposure or by the selected laser wavelength.²² As such, most literature has proposed that this aromatic bio-based source can be directly converted to graphitic structures, due to delocalized π electron clouds contained in cross-linked aromatic lignin structures. This usually do not suffer the same laser-promoted bond cleavage, unless very high laser exposure is applied, leading to drastic decomposition of the material. Because of the native presence of the aromatic structures in lignin, its conversion is not fully supported over additional aromatization, as opposed to other gLIG precursors discussed in Sec. II A 3. As such, control over the aromaticity of the synthesized structures is based on the efficiency of the laser irradiation process over the cleavage of undesirable bonds, that promote more reduced structures with less oxygen functional groups. The degree of aromatic condensation relies upon reaching temperatures that promote efficient rearrangement of aromatic structures,⁷⁹ resulting into 2D lattices composing the 3D structure of gLIG. By establishing these conversion principles, more control over the resulting properties of gLIG can be achieved and tailored to specific applications.

Another class of natural aromatic precursors explored for gLIG synthesis have been naturally sourced polycyclic heavy hydrocarbons (PHHs), such as coal, tar, pitch, and biochars.^{34,80,81} These materials present a native abundance of aromatic carbon and sp^2 hybridized chemical structures, intercalated by some content of aliphatic hydrocarbon structures. By employing laser irradiation over these substrates, the aromatic content and sp^2 concentration can be tailored from amorphous native carbon into highly ordered graphitic structures with intrinsic conductive properties, characteristic of gLIG. This conversion is different from lignin conversion in that laser irradiation promotes the annealing of native sp^2 structures and a decrease in C–H bonds present in the precursor material, without the need for additional aromatization.

3. Aliphatic bio-based sources

Aliphatic bio-based precursors for gLIG synthesis are mainly found in two forms, namely, cellulose and hemicellulose [Fig. 2(c)]. The first one is formed by a polymeric arrangement of β -1, 4-linked glucose monomers, with relatively equal amounts of carbon and oxygen in its functional groups. These polymeric arrangements are then connected by hydrogen bonds between oxygen functional groups both at intra and intermolecular levels, to form more complex structures such as fibrils and fibers in wood biomass and other materials such as paper.⁸² Similarly, hemicelluloses are composed of an arrangement of multiple sugar monomers, including glucose, galactose, mannose, xylose, and other sugar residues, in heteropolymer structures with higher complexity when compared to cellulose, being found with different compositions, usually lacking the crystallinity and fibrous nature found in cellulose.⁸³

Regarding conversion mechanisms, laser irradiation of aliphatic precursors causes the same breaking of C–H, C–O–C, and C–C bonds in their structure, through photothermal or photochemical phenomena, with rearrangement of the remaining elements depending on the imposed temperature determined by the laser fluence.⁴² When compared to aromatic gLIG precursors, aliphatic ones do not possess the necessary, native aromatic ring structures with sp^2 hybridized carbon bonds. Thus, they require a higher degree of laser exposure to achieve similar degrees of graphitization reached by aromatic precursors. Because of this, many authors have proposed that for these aliphatic sources to be converted to graphene lattices and gLIG structures, a first step of carbonization is required. Thus, there is the formation of more amorphous char structures, in opposition to a direct graphitization process, verified when using aromatic precursors, such as PI or lignin.^{50,68} In complex natural materials, where there is a simultaneous presence of aromatic and aliphatic components, such as in wood, it has been reported that a single step irradiation of the substrate is sufficient for gLIG synthesis, depending on laser source and irradiation atmosphere. This is because there is a synergistic effect of the two types of precursors in the conversion, decreasing the thermal and energy barriers necessary for significant rearrangement and vacancy filling of carbon bonds into sp^2 hybridized structures.⁴³ The presence of aliphatic components can also be mobilized to form conjugated interconnections among aromatic sheets in the synthesized aromatic clusters, as shown in PHHs irradiation.⁸¹

However, for substrates with high degree of aliphatic composition, such as various types of engineered paper substrates, some

impediments are imposed to direct substrate graphitization. These include not only the lack of the native aromatic compounds, but also the resulting inherent thermal resistance, that does not withstand the very high localized temperatures upon laser irradiation processes. As such, authors have resorted to the application of different chemical treatments, that promote the increase in thermal resistance of the precursor material, for example, using fire retardant chemicals or promoting oxidation reactions.^{31,42,84} Such treatments increase the thermal resistance of substrates, introducing functional groups or external molecules, such as phosphate and boron moieties, that suffer endothermic decomposition and act as chemical heat sinks, that allow for laser induced reactions to occur at the molecular level, without ignition and ablation of the precursor materials.^{85,86} If such pretreatments are not applied, most aliphatic rich substrates suffer pyrolytic decomposition processes that cause the formation of volatile compounds and the complete ablation of the substrates.⁸⁷ Contrarily, when such pretreatments are applied, the aliphatic rings in cellulose will undergo pyrolytic modification caused by the imposed laser photon energies and high temperatures, with different stages that lead to the formation of sp^2 rich carbon structures characteristic of gLIG.

For photodegradation of cellulose and hemicellulose structures, radiation with different wavelengths mainly causes depolymerization of polymeric chains, by scission of C–O–C glycosidic bonds, or photo-oxidative degradation, that can lead to the formation of reactive radicals.⁶⁴ Depending on the laser fluence, higher wavelengths near the IR can also cause cross-linking and the formation of new chemical species that possess sp^2 hybridization, such as furfural, that can have interesting properties, such as high fluorescence.^{64,88} Also, the tailoring of laser photon wavelength to specific vibration modes in specific bonds can be used for their cleavage.⁵⁹

In terms of thermochemical effects arising from pyrolysis of cellulose and hemicellulose through different methodologies, the exposure of these polysaccharides to high temperatures causes depolymerization of sugar monomers and subsequent decarboxylation, aromatization, and intramolecular condensation of the resulting aromatic structures.^{89–91} Some pyrolysis methods have been used for the synthesis of PAHs from cellulose and hemicellulose, showing the possibility to transform the aliphatic ring structures characteristic of these polysaccharides into aromatic rich chemical structures.^{92,93} These aromatization mechanisms are based on the thermal decomposition of cellulose and hemicellulose, to form intermediate species such as furan and furfural, that already contain some degree of sp^2 hybridization.⁹⁴ Further thermal decomposition also leads to the synthesis of carbon pools composed of hydrocarbons with C=C bonds, such as ethene, propylene, or butene. This can take part in cyclization reactions for aromatization and recyclization for the extension of these aromatic chemical structures, ultimately leading to the synthesis of chars and graphitic structures. As such, laser irradiation processes for conversion of these precursors into gLIG is modeled by the same reactions happening in the fast time frames of laser pulse irradiation, namely: (i) photochemical and/or photothermal promoted dehydration and decarboxylation of aliphatic ring structures, that leads to depolymerization by cleavage of C–O–C glycosidic bonds into D-glucopyranose or other sugar monomers, followed by (ii) deoxygenation and dehydration, through cleavage of C–O, C–H, and C–C bonds and rearrangement of carbon atoms into sp^2 rich chemical structures, by cyclization, serving as the template for aromatization and producing H_2O , CO, and CO_2 .

Finally, the high temperatures imposed by the laser irradiation allow for (iii) aromatization and intramolecular condensation, for the rearrangement of aromatic rings into sp^2 dominated graphitic structures [Fig. 2(e)]. It is important to note that such reactions happen extremely fast when compared to other pyrolytic biomass treatment methods, due to the pulsed nature of most laser conversion methods and the very high temperatures that can be reached, being extremely hard to model how each of these steps influence the formation of gLIG structures from aliphatic precursors. In this case, it is important to select laser operational parameters achievable high degrees of depolymerization and aromatization, while simultaneously allowing for the necessary intramolecular condensation into aromatic-rich structures and possibly polycondensation of these structures into larger 2D lattices composing 3D gLIG structures.⁹⁵ Therefore, due to the lack of native aromatic rings in these precursors, the additional aromatization step changes the dynamics of the conversion when compared to aromatic precursors. Consequently, many authors have reported that single step irradiation processes of aliphatic rich substrates lead to carbonization, forming chars with the significant presence of oxygen moieties, similar to graphene/graphite oxide.^{42,67} Because of this phenomenon of initial carbonization and char formation, many authors have suggested that for gLIG synthesis to occur, there needs to be a multiple lasing scan approach. This process leads to a progressive breaking and rearrangement of carbon bonds from the native aliphatic rings to chars until reaching graphene like structures with very high carbon content and negligible carbon-oxygen bonds. However, this process can also be replicated by manipulating laser operational conditions, such as the lasing power, pulse resolution, and the laser spot size upon irradiation, to increase bond breaking efficiency and create pulse overlapping patterns that mimic multiple lasing approaches.⁴⁷

This is also important when considering the use of low wavelength laser sources, such as UV lasers, since these may have different interaction dynamics between the laser beam and the substrate. While a limited number of studies have reported the application of alternative laser sources for gLIG synthesis in high cellulosic content substrates,⁴⁷ these introduce important aspects, such as if the radiation absorption of the substrate is compatible with the specific wavelength of the laser source. Thus, this conversion process presents a very dynamic phenomenon, that can be manipulated in many ways with the purpose of achieving tailored physical, chemical, and conductive properties for each target application. In addition, understanding the dynamics associated with both aromatic and aliphatic gLIG precursors may lead to future improvement on the development of green composite materials, that can assimilate the advantages of both types of precursors, similarly to raw materials such as wood. This would potentiate the efficiency of the discussed graphitization processes, ensuring better sp^2 hybridization yield and maximizing specific properties for different target applications, as discussed in Sec. II B.

B. Physical, chemical, and conductive properties of green LIG

When assessing the quality and composition of graphene synthesized by different methods, various characterization techniques are complementary employed to evaluate several key aspects of the 2D structure of the material. Similarly, the same characterization techniques have been used to study and optimize the synthesis of gLIG in

bio-based carbon substrates and correlate the laser operational parameters with different outcomes and properties upon the laser irradiation process, as summarized in Fig. 3.

1. Raman spectroscopy characterization of green LIG

Raman spectroscopy is the prevalent characterization performed for gLIG assessment, by tracking the characteristic graphitic peaks and their intercorrelation. The characteristic Raman spectra peaks correlated with LIG are D ($\sim 1320\text{ cm}^{-1}$), G ($\sim 1575\text{ cm}^{-1}$), and 2D ($\sim 2645\text{ cm}^{-1}$), where these bands represent defects in graphene lattices, the degree of graphitization and the degree of crystallinity and arrangement of graphene layers, respectively.^{69,96,97} Several authors have shown that these peaks present variations depending on the laser parameters used for synthesis, shaping the resulting conductive properties of 3D gLIG patterns. Depending on laser power, lasing scan speed, and other important variables such as laser spot size, pulse resolution, or number of lasing scans, the efficiency of the conversion processes described before can be manipulated, to achieve different peak profiles, that can be like graphene oxide structures, evolving to profiles similar to stacked graphene or graphite. The most widely studied variable and its influence on the Raman profile of LIG patterns has been the energy employed to the surface of the native substrate. This energy is usually represented by the laser power used in the laser source. Alternatively, laser fluence has been considered, because it takes into consideration different energy density profiles that influence the resolution and efficiency of the conversion. Several authors have shown that a progressive increase in this energy or in the laser power leads to more desirable outcomes in terms of the Raman profiles [Fig. 3(a)]. As shown by Jeong *et al.* and Ye *et al.*, manipulation of the laser fluence leads to different Raman profiles with varying intensities of its characteristic peaks, showing the synthesis of more amorphous structures for lower input energies, in opposition to graphitic structures for increased fluences.^{43,98} A very interesting aspect also highlighted by these authors relates to the types of wood employed for gLIG synthesis and how its composition influences the resulting graphitization and Raman profile. A comparison of Raman profiles of different wood sources, such as pine (P-LIG-70), birch (B-LIG-70), or oak (O-LIG-70), shows variations in peak intensities and the resulting peak intensity ratios for the same synthesis conditions [Fig. 3(b)]. This is related to the relative composition of aliphatic and aromatic components in the wood, as shown by Ye *et al.*, confirming that the increased presence of aromatic components arising from higher lignin natural content, leads to more desirable Raman profiles.⁴³

When it comes to more isolated sources of gLIG, namely, lignin or cellulose, the same pattern of increasing the input energy for more conductive graphitization has been observed. For aromatic carbon rich gLIG precursors, such as lignin, Qu *et al.* showed that progressive increases in the laser source power leads to less intense D peaks and decreased I_D/I_G ratios, proving a very low defect density in the formed graphitic structures [Fig. 3(c)].⁹⁹ This is also accompanied by increases in the 2D peak intensity, proving the more efficient synthesis of multi-layered graphene structures, in opposition to more amorphous structures. In comparison, for aliphatic sources, such as cellulose, Park *et al.* studied this phenomenon for different laser powers and the number of laser scans performed over the substrate, finding the characteristic peaks with different intensities and ratios between them [Fig. 3(d)].⁶⁷

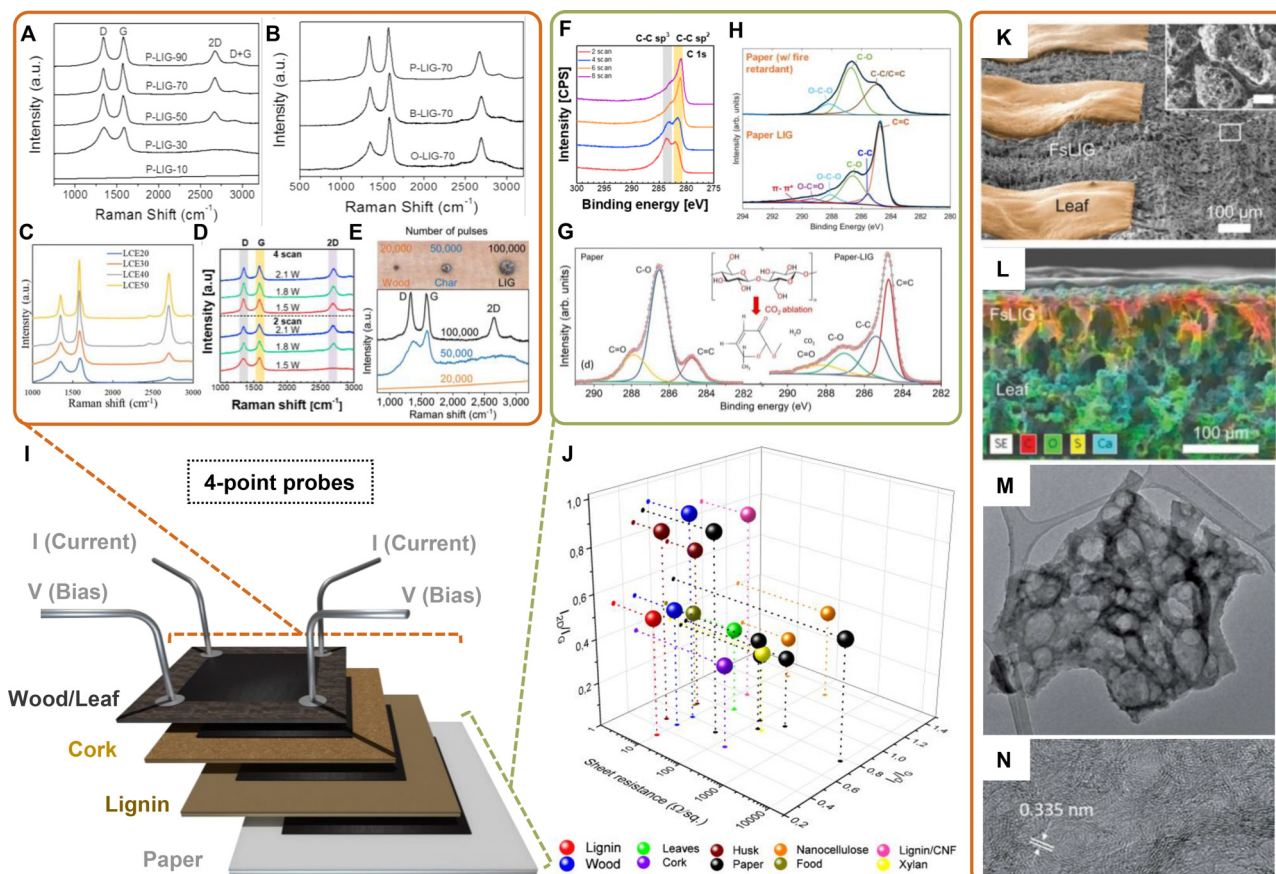


FIG. 3. Overview of physical and chemical properties of green LIG. (a) Laser powers effect on Raman spectra of natural wood and (b) influence of natural wood compositions on characteristics Raman peaks of LIG. Reproduced with permission from Ye *et al.*, *Adv. Mater.* **29**, 1702211 (2017). Copyright 2017 John Wiley and Sons.⁴³ (c) Correlation with laser powers and Raman spectra of lignin. Reproduced with permission from Qu *et al.*, *Sustainable Energy Fuels* **5**, 3744 (2021). Copyright 2021 Royal Society of Chemistry.⁹⁹ (d) Number of laser scans and laser powers influence on Raman spectra of paper. Reproduced with permission from Park *et al.*, *ACS Appl. Nano Mater.* **3**, 6899 (2020). Copyright 2020 American Chemical Society.⁶⁷ (e) Interdependence of laser pulses irradiated on the natural wood substrate and characteristics of Raman peaks of LIG. Reproduced with permission from Le *et al.*, *Adv. Funct. Mater.* **29**, 1902771 (2019). Copyright 2019 John Wiley and Sons.³⁸ (f) Influence of laser scans on XPS spectra of paper. Reproduced with permission from Park *et al.*, *ACS Appl. Nano Mater.* **3**, 6899 (2020). Copyright 2020 American Chemical Society.⁶⁷ (g) Variation of XPS spectra when the paper substrate is transformed to paper-LIG. Reproduced with permission from Zhao *et al.*, *Nano Energy* **75**, 104958 (2020). Copyright 2020 Elsevier.⁵⁰ (h) Evolution of XPS spectra of paper before and after laser irradiation highlighted the $\pi-\pi^*$ peak related to LIG conductivity. Reproduced with permission from Kulyk *et al.*, *ACS Appl. Mater. Interfaces* **13**, 10210 (2021). Copyright 2020 American Chemical Society.⁴⁹ (i) Schematic illustration of four-point probes used for measured sheet resistance of LIG-square synthesized on bio-based carbon substrates. (j) Three-dimensional graph correlated with characteristics Raman peaks of LIG with sheet resistance of several bio-based carbon substrates. (k) Colored SEM image of LIG electrodes and leaf interface highlighted a hierarchical microstructure of green LIG. (l) Cross-sectional SEM image combined with EDS map of LIG obtained on leaf substrate.⁴¹ Reproduced with permission from Le *et al.*, *Adv. Funct. Mater.* **32**, 2107768 (2022). Copyright 2022 John Wiley and Sons.⁴¹ (m) TEM image of morphology and structure of green LIG flake obtained from lignin. (n) TEM image of lattice space corresponding to the (002) plane of lignin-LIG. Reproduced with permission from Mahmood *et al.*, *RSC Adv.* **9**, 22713 (2019). Copyright 2019 Royal Society of Chemistry.¹⁰²

The authors showed that for lower laser powers and the number of laser scans, the only distinct peaks in the Raman profile are the D and G peaks, with the absence of the 2D peak, with spectra similar to amorphous carbon or GO. This evidence was also reported by other authors, showing that for low power or input energy, there is no appearance of the 2D peak and there is a preponderance of the D peak over the G peak, given by I_D/I_G ratios above 1.^{45,49} This is based on the additional aromatization step required for gLIG synthesis from aliphatic precursors, that increases the required laser energy input to achieve higher degrees of graphitization. Standing on this circumstance, authors usually resorted to increasing this input energy, to

achieve more desirable Raman profiles and conductive properties, achieving progression in the appearance and increase in 2D peak intensity, similar to that of GO reduction. This is also paired with a decrease in the preponderance of the D peak, leading to less defects in the 2D lattices composing the 3D gLIG patterns.¹⁰⁰ Indeed, Park *et al.* and other authors have reported that for increasing laser source powers, that can go from 2 to 5 W, depending on other operational variables and substrate modifications, there is a progressive increase in 2D peak intensity.^{45,67} Due to this phenomenon, authors have reported increases in the conductive properties of the resulting gLIG patterns, since higher concentrations of highly conductive aromatic

carbon rings characteristic of these graphenic structures are synthesized.^{45,47,49,67,84}

In addition to the overall energy applied to the substrates, another approach used to study the conversion mechanisms and the Raman spectra outcome when synthesizing gLIG has been through the manipulation of pulse distribution. Depending on the laser system and wavelength used for substrate irradiation, parameters such as the number of pulses or switching frequencies can be manipulated and be useful to achieve more desirable outcomes in terms of Raman profiles and conductive properties. In materials such as wood, when using short duration pulse laser systems, such as femtosecond lasers, the high photon energies require a careful manipulation of repetition rate and pulse fluence, to achieve the desired conversion outcomes. As shown by Le *et al.*, the number of pulses required for graphitization needs to be carefully studied, with Raman profiles containing the indicative D and 2D peaks in opposition to profile indicative of amorphous chars [Fig. 3(e)].³⁸ Similarly, Kulyk *et al.*, showed that q-switching frequency of a UV laser source used for gLIG conversion of cellulosic paper substrates influences the peak broadness, mainly in D and G peaks and the appearance of the 2D peak with more or less symmetry and intensity, showing similar effects to the increase in input energy.¹⁰¹ This is mainly due to the overlapping pulse patterns for high frequency regimens, that lead to increased efficiency of conversion.³⁸ In cases of the excessive overlapping, destructive phenomena over the substrates can occur, causing undesirable outcomes in terms of Raman profiles and conductive properties. In this case, the authors reported better conductive properties in the patterns for lower q-switching frequencies (40–50 kHz), associated with more desirable Raman patterns. These are interesting results, that show that these often-overlooked variables could be considered when designing mechanistic studies that help support the synthesis and characterization of gLIG for different applications.

2. X-ray photoelectron spectroscopy (XPS) characterization of green LIG

Another very important technique usually employed for the assessment of chemical features in LIG is x-ray photoelectron spectroscopy (XPS), used to study the degree of conversion of the native substrate into the necessary sp^2 hybridized conductive carbon patterns. Most authors have reported that upon gLIG synthesis, there is a characteristic appearance of strong peaks related to this hybridization in the C1s deconvoluted spectra after laser irradiation and conversion,^{49,50,67,102,103} with different degrees of intensity related to the laser parameters used in the synthesis. Such phenomenon has been verified by Park *et al.*, showing that increases in energy input for conversion, by additional lasing scans for patterning, lead to a shift in the prevalence of the C–C sp^3 peak to the C–C/C=C sp^2 peak [Fig. 3(f)].⁶⁷ For a lower number of lasing scans, there is a negligible influence of the sp^2 hybridization, giving further proof of the formation of more amorphous chars, with the characteristic Raman profiles absent of 2D peak. For a progressive increase in the number of lasing scans, there is a progressive increase in the intensity of the sp^2 -related peak, showing the more efficient conversion of the cellulosic substrate. Another important aspect of gLIG tracked by XPS is the presence and preponderance of the carbon–oxygen bonds, both in C–O and C=O forms. For different types of substrates, these bonds usually appear as very intense,

usually with the peak associated with C–O showing the highest intensity amongst the deconvoluted peaks. After irradiation, there is an expected decrease in their intensity, with this C–O peak being replaced by C–C/C=C sp^2 hybridization peak as the most count intensive,^{49,50} as expected by the break of these types of bonds during the photothermal and photochemical conversion processes [Fig. 3(g)]. Another interesting aspect related to XPS characterization reported by some authors is the appearance of π - π^* satellite peak,^{45,49} which is also related to the sp^2 hybridization, giving rise to both σ orbitals and the π orbitals responsible for the high conductivity in graphenic materials, through their delocalized electrons [Fig. 3(h)]. These peaks are not generally studied in the XPS spectra of gLIG samples, but their presence gives an indication that the synthesized material is not an insulator and is able to conduct and be applied for electrode fabrication, further confirming the graphitization processes upon laser irradiation.¹⁰⁴ Concurrently, an important aspect usually assessed using XPS has also been the relative elemental content of the converted material, more specifically in terms of the carbon and oxygen content ratio. Paired with the increase in intensity of the XPS peak related to sp^2 hybridization, the relative percentage of carbon has been shown to increase, while the oxygen content is reduced. This evidence has been demonstrated both by XPS but also through energy dispersive x-ray spectroscopy (EDS), showing that these relative elemental compositions can achieve values above 80% carbon content depending on the initial composition of the substrate, with oxygen content dropping below 20%, when compared to the high oxygen content of the native precursor materials.^{43,45,102}

3. Electrical conductivity of green LIG

Raman and XPS fingerprints, that shape the elemental and chemical properties of gLIG, also influence the conductive properties of this material. gLIG films and patterns synthesized from different native materials present tunable conductivities, depending on the synthesis conditions, that correlate them to the previously discussed chemical properties, assessed by monitoring Raman peaks, carbon hybridization and relative carbon/oxygen content. The main parameter used for the determination of gLIG conductivity, similarly to LIG synthesized from other plastic polymers, has been the resulting sheet resistance. It is important to note that sheet resistance of LIG can be measured by four-point probe method, depositing metallic contacts in the corner of the graphene square [Fig. 3(i)]. Because of the natural three-dimensional, fibrous structure of the native materials used for gLIG synthesis and the resulting hierarchical highly porous graphitic structures that ensure laser irradiation, non-uniform thickness of resulting thin gLIG films may not be conducive for accurate resistivity ($\Omega\text{ m}^{-1}$) or conductivity (S m^{-1}) assessment. When analyzing the sheet resistance of gLIG [Fig. 3(j)], it is possible to discern that raw, non-processed sources, such as wood, husks, and leaves, usually present lower values, around $10\ \Omega\ \text{sq}^{-1}$ for wood and $23\ \Omega\ \text{sq}^{-1}$ for leaf-derived gLIG.^{41,43} These more complexly structured materials retain all the aromatic and aliphatic precursors, being more easily converted to ordered, conductive graphene lattices by reorganization of both these types of carbon rings. Nonetheless, manipulation of laser parameters controlling the degree of graphitization can be used to tune sheet resistance, with the possibility of synthesizing films with values within 3 orders of magnitude above these values.⁴³

In comparison, other sources of gLIG can yield films with sheet resistance close to that of these natural sources. Reports on lignin-based gLIG films have reached values as low as $10 \Omega \text{ sq}^{-1}$,³³ showing the potential of natural, aromatic rich precursors to synthesize highly conductive gLIG patterns. Regarding aliphatic precursors, namely, cellulosic substrates, these have shown to be lacking in terms of achieving single-digit sheet-resistance values. Because of the absence of aromatic rings, these substrates need more laser exposure to achieve higher degrees of sp^2 hybridization and lower defect densities, as previously discussed, ultimately leading to less conductive films. From recent reports, sheet resistance obtained from laser irradiation of substrates, such as cardboard or chromatography paper, has reached values as low as $50 \Omega \text{ sq}^{-1}$.^{45,49} Nevertheless, resorting to the potential of paper for modification and treatments, some authors have been able to shift these sheet resistances closer to other sources, reaching values as low as $30 \Omega \text{ sq}^{-1}$.¹⁰⁵ This shows that with the further study of modification strategies of these aliphatic-based precursors, more conductive patterns can be reached.¹⁰⁶ Correlating sheet resistance to characteristic Raman peaks of gLIG [also presented in Fig. 3(j)], it is possible to observe that gLIG based on cellulosic substrates generally presents more intense D peaks, usually surpassing G peak intensity, associating graphene defects to electrical properties of gLIG obtained from carbohydrates. When compared to gLIG synthesized from lignin or more complex structural materials that contain this aromatic carbon source, the intensity of the D peak can reach much lower values and the 2D peak becomes more preponderant, combining a less defect dense graphenic structure to lower sheet resistance. According to the literature, the lowest I_D/I_G values achieved for cellulose-based gLIG without any modification other than fire retardant chemical treatments, have been around 0.7,^{47,105,107} showing that the Raman spectra in these materials usually lack low defect density, which is characteristic of graphene synthesized using other methods. This can be explained by the more complex conversion mechanism, that requires efficient aromatization of aliphatic structures and condensation into packed aromatic lattices. This may lead to higher degree of pentagonal carbon organization caused by deficient aromatization or other defects caused by the condensation processes within the crystalline 2D organization. In opposition, lignin-based gLIG has been reported to achieve I_D/I_G ratios more than twice as low as that achieved by cellulose conversion.^{99,108} The same evidence has also been shown in gLIG synthesized from wood, due to the presence of these native aromatic carbon rings.⁴³ To improve the outcomes in terms of high defect density correlated with high sheet resistance, the approach of increasing input energy has been employed, resulting in less preponderant D peaks in the Raman profile.^{38,84} Nonetheless, this improvement is achieved only until an optimal point, after which the substrate and synthesized gLIG suffer degradation and ablation processes that become dominant over the conversion, due to excessive energy absorption, ultimately deteriorating gLIG chemical structures. Nevertheless, the defect density profiles of gLIG from different precursors is in accordance with the nature of the volume transformation and conversion of native chemical structures, that happens at different depth levels and in extended areas, leading to the important contribution of defects not only at the hexagonal organization of carbon in the lattices but also possible crystalline-like defect formations found both in the extent of the nanosized carbon sheets and at edge sites.¹⁰⁹ Furthermore, due to this complex, anisotropic 3D native structure of these natural precursors, the

distribution of Raman features over the area of patterned gLIG can vary, showing higher or lower defect densities, depending on the measurement location.^{43,45,110} Another important consideration when determining the defect density and profile of D peak in gLIG samples is the excitation laser selected for this task. As previously demonstrated for the characterization of defects in graphene samples, the value of the ratios between D and G peaks can be highly dependent on the excitation laser used for the Raman measurement.¹¹¹ Thus, drawing comparisons between different reports can be misleading to establish the expected outcomes after synthesis, with the appropriate approach being to perform specific mechanistic studies on these properties that can serve as a guide for future work in the synthesis and optimization of gLIG.

4. Morphological characterization of green LIG

In relation to morphological characterization, scanning electron microscopy (SEM) images of gLIG/substrate permit to observe gLIG microporosity and its interface with the substrate [Fig. 3(k)]. This is important when trying to correlate different irradiation parameters to the resulting surface morphology and depth conversion, that influence electron transportation and resulting conductive properties. Due to the formation of volatiles and rapid vaporization of humidity present at the precursor substrate, the applied laser fluence and resulting temperature have a synergistic effect with the irradiation atmospheres to produce stable graphene structures.⁴³ Associating SEM images to EDS analysis, it is possible to observe the hierarchical structure of gLIG within its native substrate, combined to the elemental distribution along the cross-section of the gLIG/substrate [Fig. 3(l)], revealing in detail the laser parameters effect on morphological and chemical composition of gLIG along the substrate.⁴¹ Also aiming at gLIG nanostructure characterization, transmission electron microscopy (TEM) is a strong tool to describe gLIG flakes, revealing its few-layer features.^{28,102} TEM micrographs can expose the mesoporous and ripple-like wrinkled structures contained in gLIG flakes' surface, showing the creation of free paths targeting full functionalization of gLIG micro- and nanostructures [Fig. 3(m)].^{112,113} It is important to note that the formation of such structures is attributed to thermal expansion promoted by laser irradiation which forms an ultra-polycrystalline structure with disordered-grain boundaries.¹¹⁴ In combination with x-ray diffraction (XRD) analysis, it is possible to analyze the average lattice space corresponding to the (002) plane, indicative of the increase in crystallinity index (I_C) of gLIG [Fig. 3(n)]. The increased I_C can also be correlated with defects dispersed in the hexagonal layers of the graphene represented by the (100) plane, which could also indicate the high degree of substrate graphitization, in accordance with the crystalline size determined by XRD analysis.²⁸

III. TECHNOLOGICAL APPLICATIONS FOR GREEN LIG

Regarding the environmental issues raised by e-waste, gLIG may pave the way for simple, sustainable, and low-cost electronic devices, based on abundant and renewable bio-based carbon sources. The past few years have witnessed increasingly extensive research around gLIG for integration in various electronic applications, such as supercapacitors, sensors, electrocatalysts and triboelectric nanogenerators.^{36,38,43} As previously described, the quality of the gLIG produced, in addition to being correlated with the laser parameters used in its production, is also conditioned by the type of substrate used.⁴² These can range from

(i) raw materials extracted from natural sources, such as wood, leaves, cork and coal, to (ii) processed by-products extracted from (i), such as lignin and cellulose. Such by-products can be found in many engineered forms, ranging from lignin-rich polymeric films and composites, cellulosic substrates with different amounts of cellulose, the presence of additives and different mechanical properties, such as grammage, porosity, and pore size and thickness, to transparent nanocellulose films. Furthermore, these precursors can be combined with other chemicals to formulate inks and biocomposites, while other attractive sources, such as husks and food, have shown to be promising materials to obtain gLIG, generating high-performance electronic devices, as illustrated in Fig. 4. In this section, an overview of gLIG applications in microelectronic elements and devices is presented, according to the class of biomaterials used for its production, aiming to correlate the effect of laser conversion within each type of substrate to the fabrication and performance of several electronic devices.

A. Sources of green LIG from raw materials

The diversity of tree species on the planet makes wood, leaves, and other biomass with the varied chemical compositions, offering a plethora of characteristics to be explored. Wood corresponds to the inner structure of a tree, while leaves are mainly the stem appendages of vascular plants. They are defined by a complex hierarchical

structure of organic materials,¹¹⁵ containing 25–55 wt. % of cellulose, 10–35 wt. % of hemicellulose, and 15–45 wt. % of lignin in its composition.^{116–118} Harvesting these substrates includes cutting and processing trees, which can cause substantial damage to the forest and its soils. Alternatively, substrates such as cork are just the tree bark, more specifically derived and extracted from the *Quercus Suber L.* species, cultivated in southern Europe and predominant in Portugal. This raw material is obtained through a periodic extraction, without harming the cork oak itself and relying on a sustainable exploitation system.¹¹⁹ It has a characteristic difference in its chemical composition, which is the presence of suberin and the reduced content of hemicellulose and cellulose compared to wood and leaf substrates.¹²⁰ It was found that these natural products are converted directly into gLIG, mainly due to the lignin content present in its composition. Thus, higher lignin content is more favorable to produce better-quality gLIG,⁴³ as previously discussed, with the possibility of selecting the most appropriate raw precursor for each target application and tailoring the chemical and conductive functions of the resulting gLIG patterns.

From an environmental and economic point of view, these substrates can be one of nature's most versatile materials, with extraordinary intrinsic characteristics, such as biodegradability, impermeability, lightweight, and resistance to different thermal conditions.¹²¹ Another natural source within this class of raw materials is coal, an organic sedimentary rock rich in carbon, produced from the compaction and

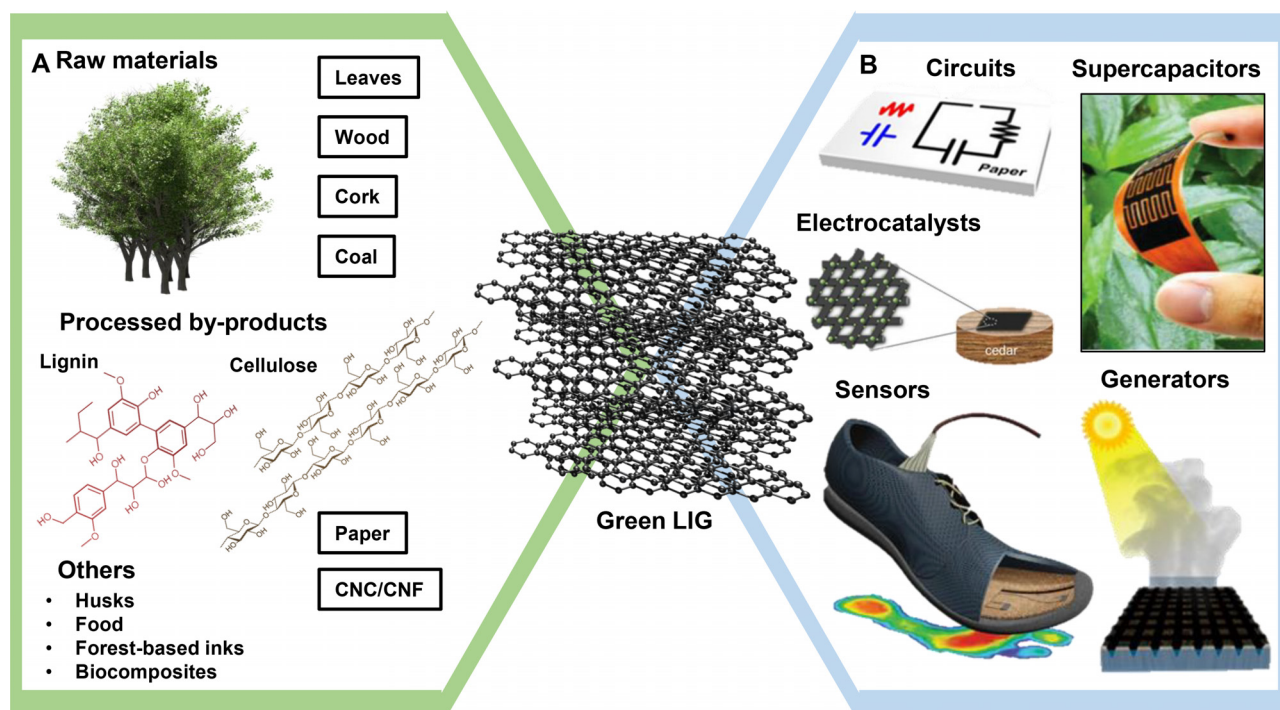


FIG. 4. Green LIG from synthesis to applications. (a) Three distinct categories are shown based on the degree of processing of the precursor before gLIG synthesis (b) Most prevalent applications for gLIG in the literature. Circuits illustrative image reproduced with permission from Park *et al.*, ACS Appl. Nano Mater. 3, 6899 (2020). Copyright 2020 American Chemical Society.⁶⁷ Supercapacitor illustrative image reproduced with permission from Le *et al.*, Adv. Funct. Mater. 32, 2107768 (2022). Copyright 2022 John Wiley and Sons.⁴¹ Electrocatalysts illustrative image reproduced with permission from Han *et al.*, ACS Appl. Nano Mater. 1, 5053 (2018). Copyright 2018 American Chemical Society.¹⁰⁶ Sensors illustrative image reproduced with permission from Carvalho *et al.*, Adv. Mater. Technol. 5, 2000630 (2020). Copyright 2020 John Wiley and Sons.¹²⁴ Generators illustrative image reproduced with permission from Jang *et al.*, ACS Appl. Mater. Interfaces 12, 30320 (2020). Copyright 2020 American Chemical Society.¹²³

hardening of altered plant remains.¹²² Nowadays, these renewable materials are used in the most diverse technological sectors and have also been exploited to produce gLIG, holding great promise for green electronics development.^{43,102} The properties of hierarchical porous graphene obtained from these bio-based carbon sources are closely correlated with substrate composition, the laser source used for gLIG conversion, laser parameters, substrate pretreatment, and gLIG doping strategies after irradiation, as discussed earlier. Figure 5 illustrates an example of each substrate with practical applications based on green gLIG.

Initially, the first report on gLIG from wood was put forward by Tour *et al.*, using a CO₂ laser under an inert atmosphere, obtaining 3D porous graphene with low sheet resistance ($\sim 10 \Omega \text{ sq}^{-1}$), leading to

the development of patterned electrodes for supercapacitors and water-splitting systems.⁴³ This approach opened the possibility to produce multifunctional wood-based hybrid materials, also showing the prospect of engineering the surface of wood substrates toward functional electronic applications. Such approaches have been reported, for example, using cedarwood, embedded with metal salts, resulting in converted porous gLIG with high conductivity ($\sim 8 \Omega \text{ sq}^{-1}$), unique ferromagnetic behavior, and excellent electrochemical catalytic performance. This approach was tested with multiple metal salt precursors, from copper to a mixture of nickel and iron, to simultaneously produced gLIG patterns and induce laser-assisted nucleation for metal nanoparticle synthesis. Thus, incorporating different inorganic structures in this type of substrate suggests the generation of gLIG

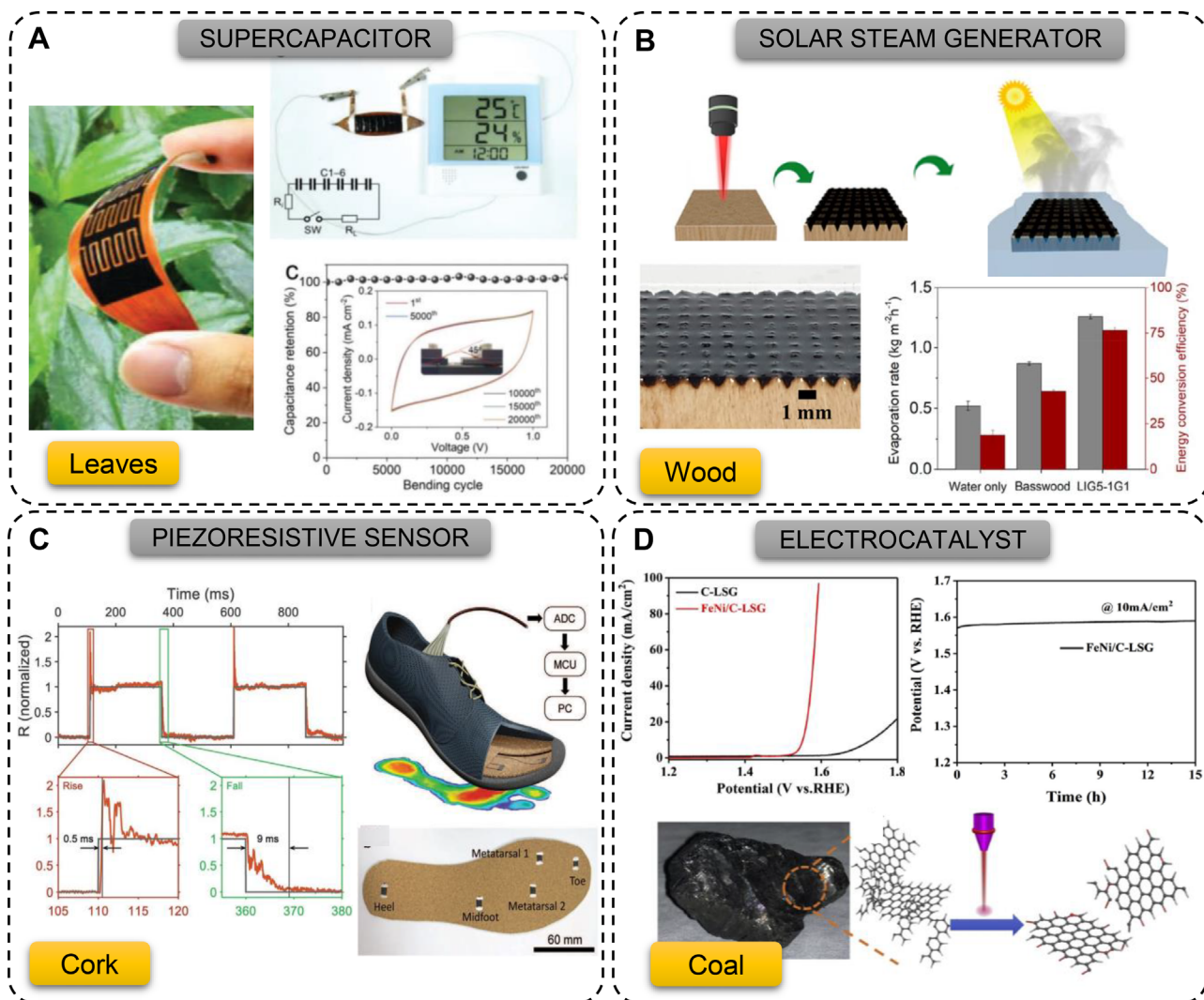


FIG. 5. Green LIG applications obtained from raw materials. (a) LIG grid pattern on basswood applied in the solar steam generator. Reproduced with permission from Le *et al.*, *Adv. Funct. Mater.* **32**, 2107768 (2022). Copyright 2022 John Wiley and Sons.⁴¹ (b) Interdigital microelectrodes based on LIG obtained from fallen leaves used in flexible supercapacitor. Reproduced with permission from Jang *et al.*, *ACS Appl. Mater. Interfaces* **12**, 30320 (2020). Copyright 2020 American Chemical Society.¹²³ (c) LIG-on-cork implemented as insole to monitor the foot pressure. Reproduced with permission from Carvalho *et al.*, *Adv. Mater. Technol.* **5**, 2000630 (2020). Copyright 2020 John Wiley and Sons.¹²⁴ (d) Electrocatalyst based on LIG synthesized from coal. Reproduced with permission from Zhang *et al.*, *Carbon* **153**, 585 (2019). Copyright 2019 Elsevier.³⁴

electrodes with improved functionalities,¹⁰⁶ opening its applicability to a myriad of electronic applications, besides simple electrode patterning. UV lasers also enabled high-resolution patterning of electronic components onto woods and leaves under ambient conditions without the use of inert gases, such as argon.^{38,41} In these works, gLIG presented similar sheet resistances to those previously reported for CO₂ laser conversion, allowing for the patterning of conductive tracks and temperature sensors on leaves, with great and fast responsiveness. Sandwich-type supercapacitors using wood-based MnO₂/gLIG electrodes have also been produced, showing higher areal capacitance (53.6 mF cm⁻² at 1 mA cm⁻²) than supercapacitor based on gLIG produced on PI.³⁸ Thus, the use of doping strategies may solve certain inherent barriers of pure gLIG in these types of natural materials. A similar work proposed that ultrashort laser pulses can benefit gLIG production on thin and thermosensitive substrates, such as natural leaves, with minimized thermal effect and ablation. Also, the presence of biominerals in leaves' composition can serve as nucleation sites for the growth of 3D mesoporous gLIG with low sheet resistance (23 Ω sq⁻¹). The development of flexible leaves-based micro-supercapacitors showed excellent electrochemical performance with high areal capacitance (34.68 mF cm⁻² at 5 mV s⁻¹) and capacitance retention (≈99% after 50 000 charge/discharge cycles) comparable to other undoped gLIG-based devices reported so far [Fig. 5(a)].⁴¹ Another interesting approach using wood substrates has been the exploitation of laser irradiation to not only induced the synthesis of graphenic structures, but also manipulate pulse profiles for surface micro structuring. Jang *et al.* used this approach to develop different gLIG grid patterns into wood, for the development of a solar steam generator (SSG) with high solar conversion efficiency, with improved salt-resistance and self-regeneration properties, promising for water desalination applications [Fig. 5(b)].¹²³ Other applications of wood-based gLIG converted using UV lasers include eco-friendly and disposable pH sensors, exhibiting an accurate pH sensitivity, for use in agriculture.⁹⁸ More recently, alternative chemical treatments on wood substrates have been proposed, to improve on some aspects of CO₂ laser conversion processes. Dreimol *et al.* presented the use of iron catalysts,¹¹⁰ with the purpose of protecting wood from excessive laser ablation and thermal damage, promoting a more efficient graphitization and smooth gLIG surfaces, without the need for multiple lasing steps, use of fire-retardants or inert atmospheres. Using an aqueous, bio-based iron-tannic acid ink for wood coating, large area gLIG surfaces were patterned in flexible wood veneers, resulting in very attractive conductive properties, with sheet resistance around 25 Ω sq⁻¹. The resulting gLIG was applied in various electronic devices, including flexible strain sensors and electrodes, wood-based touch button panels and light-emitting electroluminescent devices. This work showed the excellent multifunctionality of wood-based gLIG, patterned in different types of wood, including thin, flexible veneers, that can open the possibility to produce flexible devices for different targets.

In the literature, gLIG from natural and agglomerated cork has been demonstrated as an exciting material for on-cork electronics and wearable applications. For example, high-efficiency energy storage devices were reported in natural cork, where a 450 nm wavelength laser was used to fabricate flexible cork-based supercapacitors in both planar and sandwich configurations. Using a boron treatment prior to laser irradiation, boron-doped gLIG was synthesized, resulting in gLIG with sheet resistance of 73 Ω sq⁻¹. This strategy resulted in better

performance cork supercapacitors, when compared to undoped cork-based gLIG electrodes, with areal capacitances going from 4.67 mF cm⁻² for undoped gLIG using sandwich configuration, to 11.24 mF cm⁻² for boron-doped gLIG using the same configuration. The devices maintained good stability over time, with ~14% loss in retention for both configurations, after more than 10000 charge/discharge cycles.⁴⁶ Another interesting application for gLIG-on-cork was presented by Carvalho *et al.*, that developed sensorized insoles to monitor human gait, by the analysis of the different phases of the pressure signal for distinct foot regions. The piezoresistive sensors showed high sensitivity (up to 9.8 × 10⁻³ kPa⁻¹) and fast response time (0.5 ms rise, 9 ms fall) [Fig. 5(c)].¹²⁴ Other emerging applications can also benefit from the use of cork and its resulting gLIG, namely, energy harvesting. Highly flexible and stretchable triboelectric nanogenerators were developed, by obtaining gLIG from agglomerated cork as an additional component for power generation from human body motion. These triboelectric nanogenerators were composed of gLIG/cork bilayer composites, generating an open-circuit voltage from +35 to -105 V when in contact with a PI substrate.³⁶ By developing such energy storage and harvesting elements, in conjunction with functional sensing elements, the robust, flexible properties of cork can be used to develop multifunctional flexible and wearable electronic systems, with great versatility and added value in production chains and within a circular economy.

Coal-based gLIG is also reported in the literature, but still with much to explore. Owing to its high aromaticity and rich native carbon sp² hybridization, a multifunctional gLIG with high electrical conductivity (12 Ω sq⁻¹), high electrochemical sensitivity, and ionic storage properties has been synthesized. Coal-based gLIG showed promising applications for Joule heating (power density of 1.075 W cm² to reach ~96 °C), electrochemical sensing (limit detecting 0.5 μM for dopamine), supercapacitors (capacitance of 35 mF cm⁻² at 1 mA cm⁻²), and electrocatalyst of the oxygen reaction using FeNi hydroxide onto gLIG, with low over potential [Fig. 5(d)].³⁴ In addition to coal, other PHHs have been used to synthesize graphitic structures homologous to gLIG, as is the case of tar. Zang *et al.* studied the laser-induced graphitization of different PHHs and compared the resulting chemical and conductive properties for use in electronics.⁸⁰ Tar was then applied as a coating for PDMS flexible substrates and submitted to irradiation and patterning, for the fabrication of flexible electrodes for different applications, including transparent heaters, interdigitated supercapacitors and flexible strain sensors, with appealing performances. Coal products have also been functionalized with several dopants, aiming at modifying the resulting electronic properties and to include magnetic properties after laser graphitization processes. Using coal-Fe/Co oxide composites, laser irradiation and transfer of resulting graphitic structures into an Ecoflex substrates allowed for the fabrication of a gripper soft actuators.

These recent discoveries have paved the way for the preparation of low-cost and scalable green electronics based on gLIG from wood, leaves, cork, and coal, aiming at the development of flexible and sustainable platforms as an alternative to conventional technologies. Nowadays, gLIG from these naturally recurring materials stands out in several applications such as supercapacitors, sensors, generators, and electrocatalysts, showing promising performances compared to other green sources, as described in Table 1. The first reported works showed the potential of wood to produce gLIG due to its uniform and

TABLE I. A list of gLIG applications, substrate pretreatments and laser conditions related to raw materials. IR—infra-red, KMnO_4 —potassium permanganate, UV—ultraviolet, H_3BO_3 —boric acid, TCR—temperature coefficient of resistance.

Application	Atmosphere	Laser	Substrate	Pretreatment	Performance	Reference
Supercapacitor	Inert	IR 10.6 μm	Wood	...	1 mF cm^{-2} @ 1 mA cm^{-2}	43
				KMnO_4 solution	54 mF cm^{-2} @ 1 mA cm^{-2}	38
		UV 343–346 nm	Leaf	...	35 mF cm^{-2} @ 5 mV s^{-1} / 50 000 cycles	41
		Visible 450 nm	Cork	H_3BO_3 solution	3.7 mF cm^{-2} @ 0.1 mA cm^{-2} / 5000 cycles	46
		IR 10.6 μm	Coal	...	35 mF cm^{-2} @ 1 mA cm^{-2} / 1000 cycles	34
	Tar		...	2 mW h/cm^3 and stable cycling performance at up to 2.5 V	80	
Sensor	Air	UV 343–355 nm	Wood	...	pH ($-4.2 \text{ k}\Omega \text{ pH}^{-1}$) between 4 and 10 pH	98
			Leaf	...	Temperature (TCR -0.08% $^{\circ}\text{C}^{-1}$)	38
			Coal	...	Temperature (1.075 W cm^{-2} to reach $\sim 96.4^{\circ}\text{C}$)	34
		IR 10.6 μm	Wood	Iron–tannic acid ink	Strain sensor (sensibility 0.08 mm/mm, >69 000 cycles)	110
	Tar		...	Strain sensor (sensibility 0.01 mm/mm) and heat sensor (reach up to 300°C)	80	
	Cork		...	Mechanical (up to $9.8 \times 10^{-3} \text{ kPa}^{-1}$)	124	
Generator	...	UV 355 nm				
		IR 10.6 μm	Wood	...	0.8 kW m^{-2}	123
			Cork	...	V_{OC} from 35 to -105 V	36
Electrocatalyst	Inert		Wood	Metal ions	Over potential 0.3 V @ 10 mA cm^{-1}	106
	Air		Coal	...	Over potential 1.58 V @ 50 mA cm^{-2}	34

smooth surface, which allows an easy patterning of various desired electrode designs. However, since the ablation of wood in air can lead to the decomposition of the lignocellulose structure, complementary strategies of using an inert conversion atmosphere, pretreatments or appropriate laser wavelength selection are required steps for wood-based gLIG conversion, as showed by recent literature. Also, being a robust and bulk material limits its applicability for flexible and light-weight technology development. Even so, it holds great promise for applications in remote environments or applications where this feature is not a requirement. Leaves, in turn, could be applied to wearable devices, but processability is limited by its size and mechanical strength, as well as degradation over time. Cork appears as a promising source of gLIG, used in its natural state, as a composite, or even extracting the most useful components to be converted into gLIG. This raw material still has much to be explored, when compared with the number of works reported for wood, but the fact that this material has a high temperature resistance means that it can be converted to gLIG in different atmospheres, and consequently generate gLIG with promising features. Cork has attracted a lot of interest due to the possibility of having a hybrid material that allows flexibility, lightness, and

the production of gLIG with electrical conductivity on par with conventional gLIG precursors.

B. Sources of green LIC from processed by-products

Lignin and carbohydrates stand out as the main processed by-products for gLIG synthesis, with distinct chemical characteristics. Considering each of its particularities, lignin is the most abundant aromatic polymer in nature, being mainly obtained from wood by the Kraft process employed by the paper industry. Its branched and aromatic chemical structure guarantees its direct transformation to gLIG under ambient conditions.¹²⁵ On the other hand, carbohydrate polymers present aliphatic carbon rings that can be indirectly converted into gLIG. The main source of these chemical structures is found naturally in wood and other vegetable biomass, being found mainly in the form of cellulose and hemicellulose. However, other similar chemical structures can be abundantly found in nature and are regularly explored and transformed into other high valuable products in electronics.^{126,127} These can include starch, glycogen, chitin and other similar chemical structures, that may be transformed into graphitic

structures and thus, gLIG.^{128,129} To date, the focus on carbohydrate-based synthesis of gLIG has mainly been on cellulose-rich substrates. These take the form of differently engineered paper substrates, such as cardboard, office and chromatography papers, possessing different chemical compositions that lead to the synthesis of differentiated gLIG regarding chemical and conductive properties. In addition, other more refined forms of cellulose, such as nanocellulose crystals and fibers, have been used for gLIG synthesis, targeting different electronic applications. Considering this scenario, the main technological employment of gLIG obtained from lignin, paper and nanocellulose is reported below.

1. Lignin

As previously reported, the synthesis of gLIG can be performed directly on lignin under ambient atmosphere, inspiring future research using extracted lignin to generate green electronics.⁴² However, for neat lignin to be used in functional gLIG patterning, its blending with other polymeric materials is required, or it needs to be refined and modified into thermoset biopolymers.¹³⁰ The most common polymeric matrices used for lignin embedding have been flexible or elastomeric materials, such as polydimethylsiloxane (PDMS) or polyacrylonitrile (PAN), expanding its applicability toward flexible and wearable technology. Similarly, other materials such as cloths have been used to ingrain lignin and develop wearable, integrated components. Considering this scenario, Fig. 6 summarizes some illustrative examples of electronic devices contained lignin-based gLIG.

Originally, lignin mixed with PDMS at different wt. % was studied as an effective matrix for gLIG synthesis. The lignin modified PDMS film allowed for direct scribing of gLIG patterns using a UV laser, toward the fabrication of pressure sensors with sensitivity between 350 and 900 Pa.¹⁰⁸ A similar approach was proposed by Wang *et al.*, where lignin-PAN films doped with molybdenum disulfide (MoS_2) were employed for gLIG patterning of electrodes for supercapacitor applications, resulting in enhanced electrochemical performance. When comparing lignin-PAN MoS_2 doped and undoped films, the areal capacitance improves to 16 mF cm^{-2} at 10 mV s^{-1} .¹⁰³ Similarly, sulfur-doped porous gLIG was obtained using lignin-polyethersulfone (PES) composite films, resulting in very attractive gLIG in terms of its chemical properties. This was also translated into the fabrication of electrodes for supercapacitor applications, improving electrochemical performances up to 22 mF cm^{-2} at 0.05 mA cm^{-2} , with great stability over 8000 cycles [Fig. 6(a)],⁵¹ demonstrating the importance of lignin-based gLIG functionalization for better performance of electronic devices. Using lignin-polyethylene oxide (PEO) composite films and employing similar strategies for gLIG synthesis, Mahmood *et al.* employed electrode patterns to produce sandwich configurations, achieving a specific capacitance of 25 mF cm^{-2} at 0.1 mA cm^{-2} , revealing the importance of graphene electrode arrangements for improved supercapacitor performance.¹⁰²

A very interesting alternative approach to embed lignin into high value matrices has been the modification of cloths with this gLIG precursor. Instead of engineering composite films, authors have proposed the ingrain of lignin into different cloths, boosting their properties and embedding functional electronic elements through laser scribing. The main approach has been the deposition of lignin on carbon cloths, resulting in very attractive results regarding the chemical properties of the resulting gLIG, in terms of the defect density and conductivities of

gLIG chemical structures. This is evidenced by the good electrochemical performance of the developed microsupercapacitors, reaching maximum areal capacitance of 148.6 and 157.3 mF cm^{-2} , validating gLIG-lignin application in wearable energy storage electronics.^{99,131}

Another interesting approach for lignin-based gLIG has been the synthesis of lignin solutions and suspensions within polymeric solvents, such as polyvinyl alcohol (PVA), able to cast into a support substrate through different techniques, such as blade coating.¹³² After film casting, authors have shown the possibility to convert the films to gLIG and pattern any functional design, followed by removal of excess lignin through liftoff methodologies, leaving only the scribed gLIG patterns behind, coining this method lignin laser lithography. Based on this water-lift off technique, authors have developed gLIG patterns with sheet resistances in the $5 \text{ } \Omega \text{ sq}^{-1}$ range, very low defect density and high degree of graphene crystallinity. This very promising gLIG form was used to develop microsupercapacitors with high areal capacitance of 25.1 mF cm^{-2} , volumetric energy density of 1 mW h cm^{-3} and volumetric power density of 2 W cm^{-3} .¹³² More recently, in-plane hybrid micro-supercapacitors based on these lignin-based gLIG electrodes were constructed, using CuFe-Prussian blue analogue (CuFe-PBA) applied at the positive electrode and pseudocapacitive titanium carbide MXene ($\text{Ti}_3\text{C}_2\text{T}_x$) implemented at the negative electrode by spray coating [Fig. 6(b)]. The hybrid supercapacitors showed a capacitive behavior combination between CuFe-PBA and $\text{Ti}_3\text{C}_2\text{T}_x$ reaching a very high areal capacitance value of 198 mF cm^{-2} at 1.0 mA cm^{-2} . The hybrid supercapacitors also demonstrated a good performance over 10000 cycles retaining 62% of the original capacity.¹³³ Although the application of lignin-based gLIG has mainly focused on the development of energy storage elements in the form of microsupercapacitors, the lignin laser lithography principles have been applied for other electronic components, namely, planar electrochemical cells for application in electrochemical biosensors. Performing the same scribing and water liftoff methodologies, electrochemical cells composed of three working electrodes (WE) and common counter and reference electrodes were fabricated, for enzymatic biosensing of glucose, lactate and alcohol [Fig. 6(c)].¹³⁴ The biosensing strategy was based on the modification of the WEs with $\text{Ti}_3\text{C}_2\text{T}_x$, Prussian blue (PB) and the corresponding enzyme, capable of translating the biochemical reaction of each recognition element with the corresponding target analyte in to an electric signal. Owing to the very good electrical properties of the scribed gLIG patterns, with sheet resistance as low as $2.8 \text{ } \Omega \text{ sq}^{-1}$, high performance, on-chip biosensing of these three analytes was achieved. For glucose, glucose oxidase (GOx)-based biosensing resulted in an extended linear detection range, between $10 \text{ } \mu\text{M}$ and 5.3 mM , with a limit of detection (LOD) of $0.3 \text{ } \mu\text{M}$. For lactate, lactate-oxidase (LOx)-based detection was achieved between 0 and 20 mM , with an LOD of $0.5 \text{ } \mu\text{M}$. Finally, alcohol oxidase (AOD) modified WE reached alcohol detection in a range between 0 and 50 mM . These biosensing schemes applied in the lignin based on-chip electrochemical biosensor were tested using an artificial sweat matrix, showing the great potential for the development of wearable, biochemical monitoring systems. Thus, the lignin stands out as a promising processed by-products source for gLIG, applied mostly in supercapacitors, as evidenced in Table II. These energy storage devices present superior performance to those exhibited by raw materials. On the other hand, lignin-based gLIG is still unexplored for other applications, such as triboelectric nanogenerators and electrocatalysis,

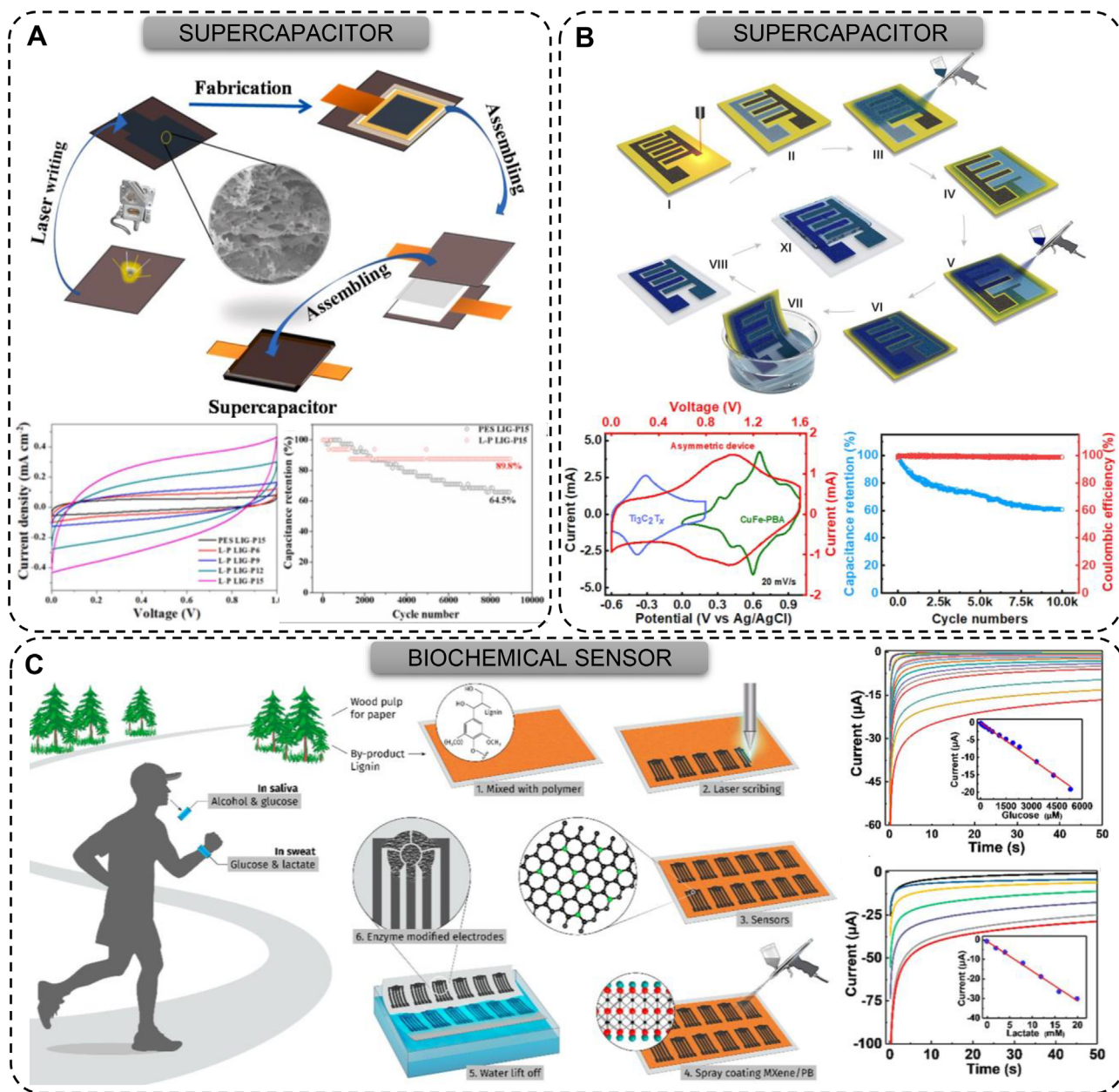


FIG. 6. Green LIG applications obtained from lignin. (a) Direct write LIG electrodes on lignin mixed with thermoplastic substrate for glucose and lactate sensing. Reproduced with permission from Sun *et al.*, *Appl. Surf. Sci.* **551**, 149438 (2021). Copyright 2021 Elsevier.⁵⁷ (b) Sulfur doped supercapacitors based on LIG synthesized from lignin blended to polyether sulfone. Reproduced with permission from Lei *et al.*, *ACS Nano* **16**, 1974 (2022). Copyright 2022 Author(s), licensed under a Creative Commons Attribution (CC-BY 4.0) License.¹³³ (c) Hybrid microsupercapacitors contained lignin-based LIG and composed of CuFe-Prussian blue analogue (CuFe-PBA) and titanium carbide MXene ($\text{Ti}_3\text{C}_2\text{T}_x$) obtained by water lift-off lithography. Reproduced with permission from Lei *et al.*, *ACS Appl. Nano Mater.* **3**, 1166 (2020). Copyright 2020 American Chemical Society.¹³⁴

showing great promise for the development of other high performance microelectronic devices.

2. Paper and nanocellulose

Paper has gained great popularity in the field of electronics in the last few decades, due to many meritorious properties. These include

inherent properties such as flexibility, porous structure, capillary capabilities for fluid transportation and dielectric aspects in terms of conductivity, but also higher accessibility in terms of production cost, being biodegradable and easily disposable.^{135–140} It is also compatible with various fabrication technologies for electronic element fabrication, while also presenting high adaptability, for example, by the possibility of folding it or using its capillary properties for chemical

TABLE II. A list of gLIG applications, substrate pretreatments or formulations, and laser conditions related to processed by-products. IR—infrared, MoS₂—molybdenum disulfide, PAN—polyacrylonitrile, UV—ultraviolet, PEO—poly(ethylene oxide), PES—polyethersulfone, PI—polyimide, PDMS—polydimethylsiloxane, PVA—polyvinyl alcohol, TMA—trimethylamine, CNC—cellulose nanocrystals, TEMPO—2,2,6,6-tetramethylpiperidine 1-oxyl radical, CNF—cellulose nanofibrils.

Application	Atmosphere	Laser	Substrate	Pretreatment or formulation	Performance	Reference	
Supercapacitor	...	UV/visible 244–785 nm		MoS ₂ and PAN binder	16 mF cm ⁻² @ 10 mV s ⁻¹ /5000 cycles	103	
				PES binder	22 mF cm ⁻² @ 0.05 mA cm ⁻² /9000 cycles	51	
		IR 10.6 μm	Lignin	PVA binder	198 mF cm ⁻² @ 1.0 mA cm ⁻² /10 000 cycles	133	
				PEO binder	25 mF cm ⁻² @ 0.1 mA cm ⁻² /4500 cycles	102	
				Carbon cloth	149 mF cm ⁻² @ 0.5 mA cm ⁻² /5000 cycles	99	
				...	157.3 mF cm ⁻² @ 0.1 mA cm ⁻² /5000 cycles	131	
		Air		Commercial fire-retardant	135 nF @ 20 Hz	67	
				Soaked with ink	14 mF cm ⁻² @ 1.0 mA cm ⁻² /11 000 cycles	37	
			UV 410–343 nm	Lignin	PI covering	0.4 mF cm ⁻² @ 10 mV s ⁻¹	30
			IR 10.6 μm		PDMS binder	Mechanical (350–900 Pa)	108
		PVA/urea binder			Sugar (0–50 mM)	134	
Sensor	...	IR 10.6 μm	Cardboard	Monoammonium phosphate	Force amplitude 0.8 N	84	
				Liquid silicone	Temperature (–0.003 Ω °C ⁻¹) Humidity (37 fF per %RH)	150	
		Air		...	Detecting temperature (resistance variation 0.15% °C ⁻¹) and TMA gas (resistance variation 0.0041% ppm ⁻¹)	155	
				UV 343 nm	PI covering	Humidity (time repeatability 200 s between 5% and 76% RH)	30
				Phosphate-based fire retardant	Strain (0.5%–1%) and bending (28–67 ms response)	49	
				Soaked with ink	Water (ΔV/V is 11.9%) Methanol (ΔV/V is 2.4%)	37	
		...	IR 10.6 μm	Paper	Sodium borate	Ammonia (0.11%–40.6%) Limit of detection 0.33%	152
					Pencil drawn	Furosemide (limit of detection of 2.4 × 10 ⁻⁷ mol l ⁻¹)	29
					Phosphate-based fire retardant	Uric acid detection (limit of 3.97 μM and a sensitivity of 0.363 μA cm ⁻² μM ⁻¹)	153
					Fire-retardant	Uric acid detection (1–1000 μM and a sensitivity of 5 μA μM ⁻¹)	154
	Inert		CNC	Sodium borate solution/wax covering	Glucose (27.24 μA mM ⁻¹ /limit of detection of 0.13 × 10 ⁻³ M)	45	
				phosphate-based fire retardant	UV (responsivity of 1 μA W ⁻¹)	31	

TABLE II. (Continued.)

Application	Atmosphere	Laser	Substrate	Pretreatment or formulation	Performance	Reference
Generator	...			TEMPO-treated	Turn on a green LED of 2 V	35
	Air		Paper	Commercial fire-retardant	$\sim 11.8 \mu\text{J cycle}^{-1}$, >12 000 energy generation cycles	50
				Soaked with ink	Turn on a LED of 2.4 V	37
				CNF	TEMPO-treated	Turn on a LED of 2 V

modifications or development of microfluidic structures.¹⁴¹ The main chemical component of most paper substrates is cellulose, since its fabrication processes are designed to purify organic materials from wood or other sources, into engineered substrates with controlled chemical composition.¹⁴² Thus, components previously addressed, such as lignin or hemicellulose, are removed in the fabrication process of many common paper substrates. Furthermore, depending on the utility of the paper substrate, there might be variations in terms of this composition, or even variations in its physical (e.g., grammage, thickness, pore sizes) and chemical properties (e.g., presence of additives).^{143,144} Due to these characteristics, paper substrates have appeared as very appealing alternatives for gLIG synthesis, since it is possible to use the cyclic, aliphatic rings present in d-glucopyranose monomers for conversion upon laser irradiation, but also have other compounds absorbed in their volume, that can promote or even modify the dynamics of the conversion processes, for more precise control of the resulting electrical and chemical properties of the synthesized gLIG, while maintaining the intrinsic physical and mechanical properties of the paper substrates.^{45,101} Nanocellulose also stands out in electronic devices development,^{145,146} being recently applied for gLIG production due to its high specific surface area, susceptible to oxidation, robust mechanical properties and optical transparency,^{147,148} thus constituting a differentiated carbohydrate substrate compared to conventional paper.³² Furthermore, the compact 3D network created by the entanglement of nanofibrils may allow for higher degrees of graphitization, due to the low oxygen permeation in its bulk volume.³² Additionally, the high crystallinity of some cellulose nanostructures can probably increase the thermal resistance of cellulose, thus, enabling graphitization.³¹ Considering this scenario, diverse electronic devices based on hierarchical gLIG obtained directly from paper, engineered paper or nanocellulose structures are presented below, as summarized in Fig. 7.

The first reports on paper-based gLIG electrodes refer to paper-board, cardboard and phenolic-paper,^{44,84,105,107,149–151} which have considerable contents of lignin and other phenolic polymers that assist the one-step laser graphitization. Using these substrates, different interesting applications have been proposed, including electrochemical paper-based analytical devices,⁴⁴ pressure and humidity sensors for human health and environmental monitoring,^{107,149,150} and gas sensors.¹⁵² The development of these components from cellulose-rich substrates stands on the good chemical and conductive properties toward the production of electrodes and electrode systems, but also through the introduction of compatible elements that expand the

functionalities of the synthesized gLIG material, as is the case of deep eutectic solvents for selective ammonia gas sensing.¹⁵²

However, the direct translation of such principles toward more refined cellulose substrates stands on their functionalization, opening up the possibility for the formation of hierarchical porous gLIG exclusively derived from cellulose fibers.^{42,47} These treatments mostly relied on fire-retardant chemical. Initial reports from Park *et al.* showed the early applications of paper-based gLIG for the development of electric elements for circuit modeling and assembly, namely, resistors and capacitors fully fabricated by laser scribing and manipulated by exploring pattern widths and designs [Fig. 7(a)].⁶⁷ Other diverse technological applications of paper-based gLIG have also started to arise, such as triboelectric nanogenerators with very high peak-to-peak voltage of around 625 V using paper-based gLIG electrodes replacing conventional Al adhesive electrodes.⁵⁰ Moisture-driven power generators that harvest energy from breath, based on an imposed C/O gradient throughout the gLIG electrode surface have also been proposed.³⁵ Temperature, humidity and mechanical sensors based on the versatile resistive properties of paper-based gLIG and on imposed changes in gLIG fibers' conformation have also emerged,^{49,101} demonstrating paper-based gLIG as a good multifunctional material. The development of electrochemical biosensors using paper-based gLIG electrodes has also been a recent research focus. For instance, planar electrodes produced on paper have been developed to monitor different metabolites, owing to the facile disposability characteristic of these substrates. Low-cost, environmentally friendly working electrodes produced from gLIG were employed in the detection of uric acid in real human urine samples, showing the compatibility for paper-based gLIG with complex matrix samples.¹⁵³ More recently, attempts have been made to correlate the conductive and chemical properties of paper-based gLIG and the resulting electrochemical properties of electrodes.¹⁵⁴ Such studies give a more in-depth understanding of the influence different irradiation regimens and resulting outcomes have on the functional properties of the material, in this case also applied for electrochemical measurements of uric acid. Other interesting application proposed for paper-based gLIG has been its use in smart packaging and mundane paper utensils. Jung *et al.* used a visible laser to directly pattern different paper surfaces, including milk cartons, paper cups and colored papers.¹⁵⁵ Using this approach, authors developed gLIG circuits, temperature and gas sensors, that were employed to monitor food spoilage, showing the applicability of gLIG for realistic chemical and thermo-sensing capabilities.

To enhance the performance and functionality of gLIG electrodes based on cellulose fibers, functionalized and coated paper surfaces can

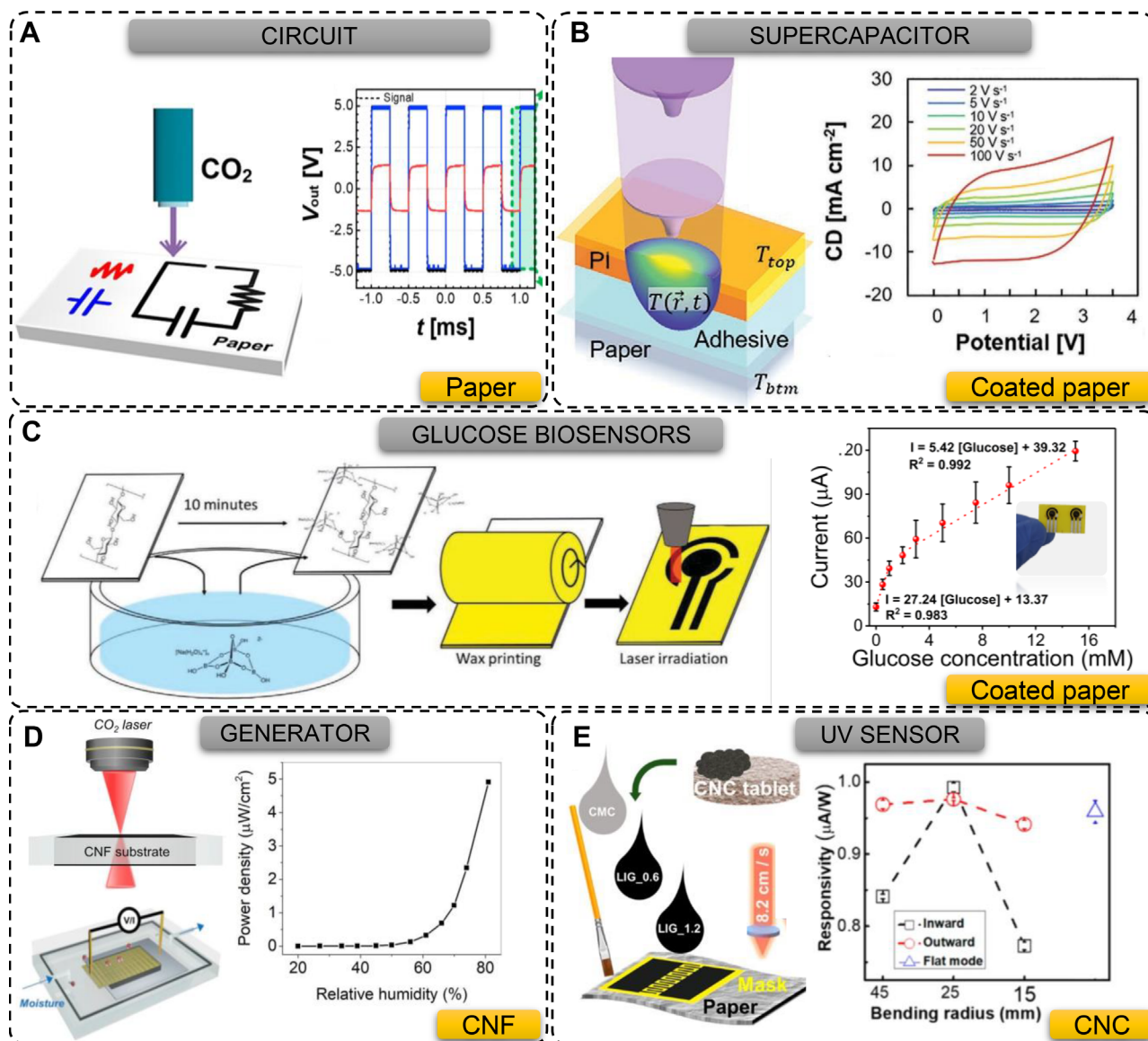


FIG. 7. Green LIG applications obtained from paper and nanocelluloses. (a) Resistors and capacitors (RC) circuit based on LIG designed on paper, highlighting the square output (blue) and inputs (red) signals of RC circuits. Reproduced with permission from Park *et al.*, ACS Appl. Nano Mater. 3, 6899 (2020). Copyright 2020 American Chemical Society.⁶⁷ (b) Thermally localized laser graphitization of coated paper with PI targeting micro-supercapacitors. Reproduced with permission from Tham *et al.*, Adv. Mater. Technol. 6, 2001156 (2021). Copyright 2021 John Wiley and Sons.³⁰ (c) Treated and impermeabilized paper with wax applied as LIG precursor and substrate in glucose biosensors. Reproduced with permission from Pinheiro *et al.*, Adv. Mater. Interfaces 8, 2101502 (2021). Copyright 2021 John Wiley and Sons.⁴⁵ (d) Moisture-driven power generator based on LIG and manufactured on CNF substrate. Reprinted with permission from Lee *et al.*, Nano Energy, 68 104364 (2020). Copyright (2020) Elsevier.⁵⁸ (e) Hand-drawn graphene electrodes on paper substrate formulated from CNC-based LIG ink aiming flexible UV oxide zinc (ZnO) sensors. Reproduced with permission from Claro *et al.*, ACS Appl. Nano Mater. 4, 8262 (2021). Copyright 2021 American Chemical Society.³¹

be developed, re-engineering its thermal and chemical characteristics, as proposed for paper soaked in solutions composed of molybdenum ions and graphite,³⁷ and pencil-drawn surface activation by laser irradiation.²⁹ Paper covered with PI tape lead to the fabrication of humidity sensors and micro-supercapacitors, fully maintaining the integrity of cellulose fibers [Fig. 7(b)].³⁰ These micro-supercapacitors showed

areal capacitances between 0.428 to 0.141 mF cm⁻² according to scan rate, showing the applicability of paper coating techniques for gLIG patterning toward energy storage devices. However, the use of PI as a coating agent removes some of the sustainability aspects of using paper as a gLIG precursor, since in this case, PI contributes to the formation of high quality gLIG. Similar strategies can be employed using other

coating agents, with improved aspects of accessibility and cost-effectiveness, while also presenting the necessary functional qualities that can improve gLIG conversion or introduce any necessary functionality. Using this strategy, wax modification and coating of borax treated chromatography paper was proposed, in order to impermeabilize the paper substrate toward the fabrication of on-chip electrochemical three-electrode cells for biosensor development [Fig. 7(c)].⁴⁵ Using these planar cells, a bi-enzymatic glucose biosensor was developed, based on WE modification with GOx and peroxidase enzymes, that resulted in an electrochemical biosensing scheme with an amperometric linear detection range between 0 and 20 mM, with an LOD of 130 μM . Owing to the versatile properties of paper, it is expected that future reports will introduce new modification methods that can improve the chemical and conductive properties of paper-based gLIG upon irradiation. These may include doping with green components that introduce aromatic chemical structures, that mimic more complex precursors, such as raw materials. Another approach may be the use of green catalysts that increase the yield of graphitization and improve several aspects such as resulting surface morphology. This has been employed by Dreimol *et al.* both in wood and in cellulose paper,¹¹⁰ using ion catalyst inks that contain an abundance of aromatic structures. By removing the need for fire retardant chemical treatments and multiple scans for graphitization, it is ensured a high conversion efficiency, while minimizing time and energy consumption in the engraving process. In fact, doping of paper substrates to introduce novel functionalities is still very much unexplored. Through modifications with inorganic components such as metallic nanoparticles and nanostructures, paper-based gLIG can be translated to novel applications in energy harvesting and storage elements, biosensing and catalysis. In addition, the very attractive mechanical and flexibility properties of paper substrates have also been unexplored in the development of multifunctional systems toward flexible and wearable technologies based on gLIG, when compared to other precursor materials such as lignin or cork.^{36,50,72}

Hierarchical porous gLIG from nanocellulose opens other diverse possibilities for obtaining structures with unique characteristics, overcoming the challenges related to directly written gLIG on paper substrate. As for example, oxidized cellulose nanofibrils (CNFs) films demonstrated that one CO_2 laser under ambient conditions was adequate to convert the CNFs, producing highly conductive graphene layers and maintaining the cellulose-based films fully intact.³² Combining these characteristics with FS lasers, a graphene 100-fold more conductive can be achieved in the CNF substrate without chemical pretreatment than the conductivity of CNF-gLIG reported previously, due to the large amount of laser pulses per time.⁷⁰ As a proof-of-concept, gLIG synthesized onto a CNF substrate demonstrated its potential as moisture-driven power generator [Fig. 7(d)], due to its sensitivity to water vapor, according to the hydrogen ions generated in gLIG-CNF interfaces.⁶⁸ This generator displayed an increase in power generation from 60% relative humidity (RH) reaching 5 $\mu\text{W cm}^{-2}$ at 80% RH. In the case of cellulose nanocrystals (CNCs), good electrically conductivity gLIG powder was synthesized from CNCs for graphene ink formulation, aiming at hand-drawn UV zinc oxide (ZnO) sensors. These sensors displayed a good performance, varying the electrical current around 7.5 μA in the presence of UV radiation [Fig. 7(e)]. The responsivity of UV ZnO sensors did not vary

significantly according to bending radius, demonstrating the efficiency of applying gLIG-based inks on flexible substrates.³¹

In this context, paper substrates, their engineered forms and nanocellulose have been demonstrated as great alternatives to enhance the performance of cellulose-based gLIG electrodes, according to their thermal resistance improvement. These developments open new promising possibilities to subtractive manufacture of electronic devices on substrates fully composed of cellulose, overcoming the challenge related to zero e-waste, paired with its great capabilities as a support substrate and its dielectric properties.^{52,67} Considering the overview of applications presented in Table II, it is possible to conclude that cellulose-based gLIG has been incorporated into diverse types of microelectronic elements, depending on imposed pretreatments and functionalization. However, gLIG made from cellulose still presents low performance in supercapacitors, when compared to raw materials and lignin, probably due to its own physical and electrical characteristics described by Raman and sheet resistance data. Thus, not only the laser parameters and the functionalization of cellulose substrates should be investigated, but the compatibilization of cellulose with other gLIG precursor materials can be an alternative to enhance the capabilities of cellulose-based gLIG in supercapacitors' performance and in other applications.

C. Other potential bio-based sources

In addition to the direct use of common raw materials from biomass sources or their abundant by-products arising from valuable and important value-chains in our society, other types of bio-based sources can be harnessed for gLIG synthesis. These include formulations containing naturally sourced components, that can act as gLIG precursors, such as forest-based inks and biocomposites, or other less abundant common materials, such as husks and food. These have shown great potential to obtain hierarchical porous gLIG by laser irradiation with very interesting properties. Forest-based inks present some prestigious characteristics of conventional inks, like their capability to be deposit on different substrates and form continuous films, being ideal mediums for the dispersion of nanoparticles.¹⁵⁶ Together with biocomposites, they can combine the characteristics of aromatic biopolymers with aliphatic biomacromolecules, promoting the synergism of properties in the graphitization of these materials.⁴⁸ Husks display a sustainable and environmentally friendly aspect as natural platforms to design gLIG profiles, due to the lignin present in their composition combined to its natural abundance.⁴² Food also represents an innovative platform to gLIG synthesis, based on concept of edible electronics,¹⁵⁷ similar to carbohydrates such as cellulose.¹⁵⁸ In this way, some illustrative examples of gLIG synthesized from these bio-based sources are presented in Fig. 8.

Citric acid and urea were used as precursor ink to fine-print conductive green gLIG circuits on a flexible substrate. These circuits presented a thin width (0.5 mm) and low electrical resistance ($\sim 1800 \Omega$), demonstrating the versatility of obtaining gLIG patterns using bio-based ink as precursor.¹⁵⁹ A related method was proposed for gLIG obtained from hydroxyethyl cellulose/lignin forest-based ink, where fine-print patterns were achieved using screen printing technique followed by laser graphitization [Fig. 8(a)]. As a proof-of-concept, a humidity sensor was developed based on these graphene patterns, exhibiting a distinct performance according to the

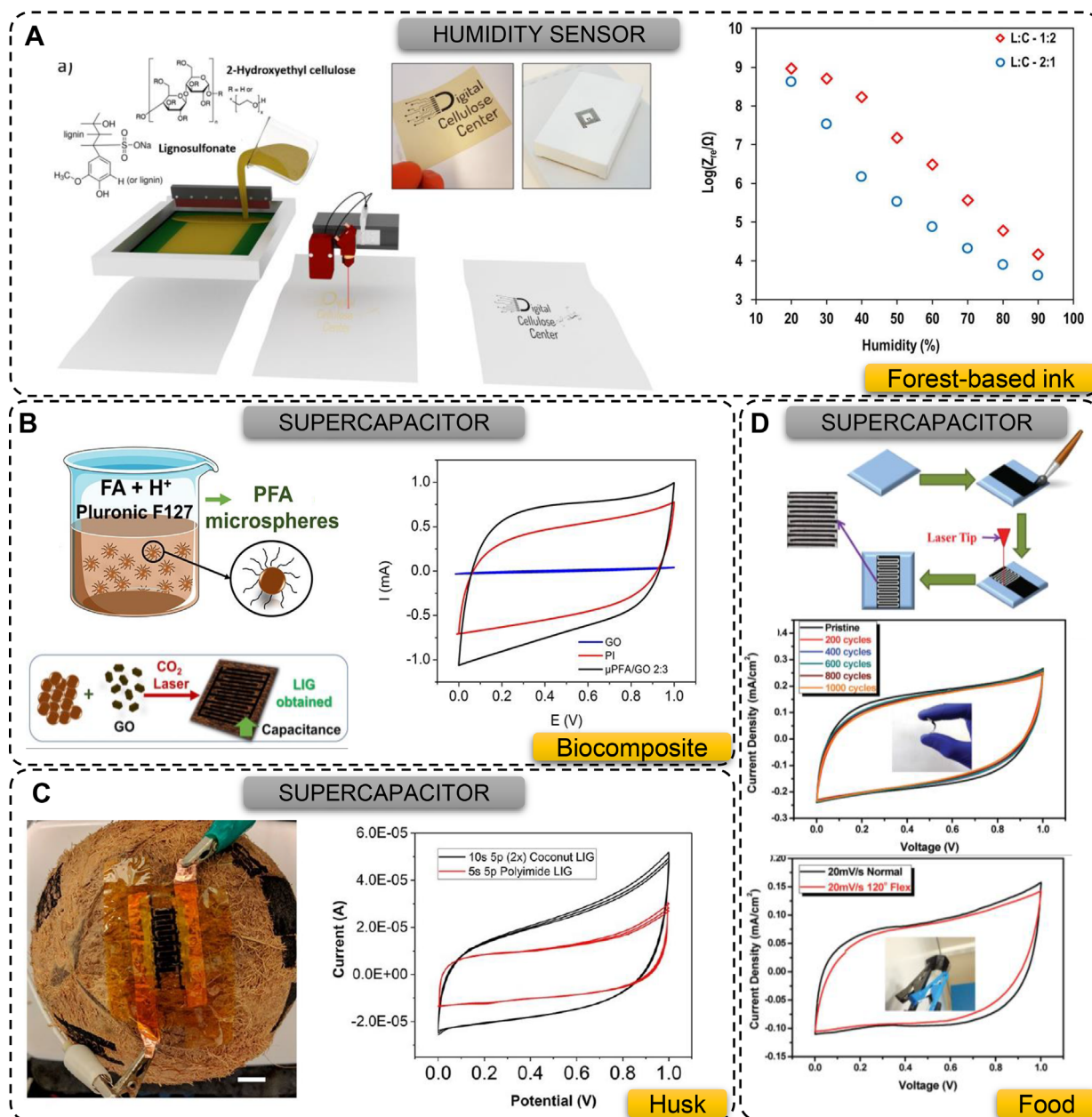


FIG. 8. Green LIG applications obtained from other potential bio-based sources. (a) Hydroxyethyl cellulose and lignin ink applied on paper by screen print technique followed by laser graphitization aiming humidity sensors. Reproduced with permission from Edberg *et al.*, npj Flexible Electron. **4**, 17 (2020). Copyright 2020 Authors, licensed under a Creative Commons Attribution (CC-BY) License.³³ (b) Poly (furfuryl alcohol) (PFA) microspheres and graphene oxide biocomposite deposited on poly (ethylene terephthalate) (PET) substrate and used as the precursor for LIG interdigital contacts applied on supercapacitor. Reproduced with permission from Hawes *et al.*, ACS Appl. Nano Mater. **2**, 6312 (2019). Copyright 2019 American Chemical Society.¹⁶¹ (c) Microsupercapacitor based on LIG interdigital synthesized on coconut husk. Reproduced with permission from Chyan *et al.*, ACS Nano **12**, 2176 (2018). Copyright 2018 American Chemical Society.⁴² (d) Mushroom-derived carbon paste deposited on PET substrate and used as LIG precursor of flexible supercapacitor. Reproduced with permission from Yadav *et al.*, Adv. Mater. Interfaces **3**, 1600057 (2016). Copyright 2016 John Wiley and Sons.³⁹

concentration ratio of lignin and cellulose derivatives.³³ Lignin-based film reinforced with nanocellulose also stood out as a promising biocomposite for gLIG electrode fabrication for electrochemical sensing, applied toward dopamine detection,⁴⁸ as well demonstrating good

potential for wearable sensor applications.¹⁶⁰ Poly (furfuryl alcohol) (PFA) microspheres obtained from waste bio-mass compatibilized with GO consolidated biocomposites as precursors for gLIG in supercapacitors [Fig. 8(b)], with devices showing areal capacitance

of 16.0 mF cm^{-2} , comparable to other energy storage devices based on GO and PI.¹⁶¹

Regarding green gLIG obtained from husks, patterns, and interdigital electrodes was obtained on potatoes and coconuts [Fig. 8(c)]. Supercapacitors based on gLIG synthesized on coconut exhibited high area capacitance comparable to the ones produced from PI, demonstrating the potential of this natural substrate for electronic devices manufacturing. However, husks are still an unexplored plant source compared to other raw materials, mainly due their own characteristics, related to their varied chemical composition and surface curvature, leading to less reproducible LIG characteristics, as reported by the authors.⁴²

Food has also become as promising source of gLIG. Initially, some gLIG patterns from food were announced on flour paste,¹⁶² toasted and as-purchased breads,⁴² presenting a similar carbonization behavior reported on cellulose. As pioneer work, supercapacitors from food-based gLIG were successfully obtained using mushroom derived carbon paste, deposited on polyethylene terephthalate (PET) substrate [Fig. 8(d)]. These supercapacitors displayed areal capacitance of 9 mF cm^{-2} at 0.5 mA cm^{-2} with great stability above 1000 cycles and on bending mode.³⁹ A similar performance was observed for supercapacitors based on gLIG synthesized from grape molasses reaching areal capacitance of 16 mF cm^{-2} at 50 mV s^{-1} due to its turbostratic structure.¹⁵⁸ Recently, studies have demonstrated that xylan also appears as a promising unexplored food carbohydrate source with great potential for gLIG formation, has demonstrated by its proof-of-concept application in temperature sensing.⁴⁷ Gelatin, a commonly available household product, has also been used for the fabrication of LIG based binder-free lithium-ion anodes. The assembled cells exhibited superior electrochemical performances and high reversible capacity.¹⁶³

Therefore, these findings establish forest-based inks, biocomposites, husks and food as promising sources for gLIG electronic device

development, aiming at several applications, as described in Table III. The chemical characteristics of these precursors require some chemical pretreatments or mixing in a polymeric matrix, allowing the graphitization process to occur in a simple way in an ambient atmosphere, applying mostly CO_2 lasers. The electronic performance of supercapacitors based on these sources are similar to the results presented for raw materials, consolidating these materials as promising gLIG precursor for energy storage devices. The same potential was observed for different sensing modalities. However, there is still a lack of studies about gLIG obtained from these precursors when compared to others bio-based carbon sources, enabling future research on new inks and biocomposite formulations as highly efficient gLIG precursors.

IV. OUTLOOK AND CHALLENGES OF ELECTRONIC DEVICES BASED ON GREEN LIG

Since its isolation in 2004, graphene has attracted much interest due to its promising physico-chemical properties. In fact, for the last decade, there has been a rush to optimize graphene production, keeping costs as low as possible while minimizing its eventual environmental impacts.¹⁶⁴ For instance, the European Union created a consortium, the Graphene Flagship, composed of 150 partners with a total budget of €1 billion. This is a huge project, covering several fields from fundamental research to long term graphene commercialization.¹⁵⁶ Similar efforts, aiming at unlocking and fully exploiting graphene's properties, are being conducted worldwide. So far, graphene has been successfully implemented in energy storage,¹⁶⁵ environmental,¹⁶⁶ biomedical applications,¹⁶⁷ among others. However, despite the tremendous investment and intense research activity, there are still many shortcomings setting back the full commercialization of graphene. Beyond cost reduction and production capacity expansion, at a more fundamental level, graphene industry faces a (i) lack of a bandgap and unavoidable defects which limits its applications; (ii) lack

TABLE III. A list of gLIG applications, substrate pretreatments and laser conditions related to other potential bio-based sources. PFA—poly (furfuryl alcohol), GO—graphite oxide, IR—infrared, PI—polyimide, PVA—polyvinyl alcohol, CNF—cellulose nanofibrils, RH—relative humidity.

Application	Atmosphere	Laser	Substrate	Pretreatment	Performance	Reference
Supercapacitor	...	IR $10.6 \mu\text{m}$	Mushroom	PVA binder	9 mF cm^{-2} @ 0.5 mA cm^{-2} / 15 000 cycles	39
	Inert		Coconut	...	Higher than PI @ 10 mV s^{-1}	42
		IR	PFA	GO addition	16 mF cm^{-2} @ 0.05 mA cm^{-2} / >10 000 cycles	161
Sensor	Air	Mid-IR $1.06 \mu\text{m}$	Grape molasses	Heat-treatment	16 mF cm^{-2} @ 50 mV s^{-1}	158
			Kraft lignin/CNF	...	Dopamine ($5\text{--}40 \mu\text{M}$)	48
	...	IR $10.6 \mu\text{m}$	Hydroxyethyl cellulose/lignin	...	Humidity (impedance spanning five orders of magnitude per RH variation)	33
			Xylan	Carboxymethyl	Temperature ($-1.29 \Omega \text{ } ^\circ\text{C}^{-1}$, range between 20 and $45 \text{ } ^\circ\text{C}$)	47
Batteries			Gelatin	Phthalocyanine	Reversible capacity of 992 mA h g^{-1} at 0.2 A g^{-1} and excellent rate capacity of 365 mA h g^{-1} at 2.0 A g^{-1}	163

of suitable sustainable production methods and “standard-grade” graphene in the market; and (iii) the inexistence of prototypes to boost and demonstrate its potential.¹⁵⁶ In fact, these aspects are interlinked with other relevant commercialization questions, namely, the perception of technological immaturity among potential investors and customers and regulatory hurdles regarding graphene toxicology and biocompatibility. Additionally, most of the advances on graphene production are still performed at university/research centers’ levels and the term “graphene” being used for many different types of products, exhibiting a wide range of properties, further creates distrust on investors and customers. These commercialization issues have been mostly addressed by optimizing and standardizing production methods. In this context, LIG has been regarded as one of the most interesting methods for graphene production. Although its properties cannot be compared to single layer graphene, LIG ease of production and handling offer many opportunities for applications that do not require the optimal properties of the available graphene powders. As it was described through this review, LIG opens the possibility for the simple, cost effective and scalable production of technological components. Since the first laser scribed conductive track, research on LIG has exponentially grown, leading to the development of sensors, supercapacitors, resistors, among others. Again, these devices do not meet the requirements and performance expected for high-end electronics but are suitable for fast-patterning flexible and wearable applications. Additionally, LIG production does not require controlled environments, expensive chemicals, or equipment, thus substantially reducing production costs, while being a sustainable and environmentally friendly subtractive manufacturing approach. It virtually produces zero waste, and it can be performed in the biocompatible and biodegradable precursor.^{25,38,41} However, LIG is not meant for powder production, eventually reducing some of its potential applications if the devices cannot be directly patterned on a substrate. On the other hand, it is a one-step manufacturing process that does not require slurry preparation or any other deposition methods, once again lowering production time and costs. Therefore, gLIG represents a very interesting and promising approach for solving, or at least reducing, the problems associated with the toxic and harmful e-waste. Additionally, gLIG is also compatible with well-established production methods, such as roll-to-roll, being poised for a quick implementation at industrial level.² Nevertheless, it is not common for new and emerging technologies to get in the market if they do not surpass the current state of the art (SOTA) or if they do not follow the “ten times cheaper or ten times better” rule.¹⁶⁸ Therefore, it is very unlikely that gLIG based devices will quickly surpass already available mature technologies, which can be produced in mass at relatively low cost. However, nanomaterials, such as graphene, exhibit clear advantages for the production and scale up of emerging flexible and wearable devices. Due to its compatibility with flexible substrates and low-cost fabrication, gLIG-based electronics can bring electronic functionality to markets unfit for rigid and expensive silicon electronics.¹⁶⁹ The technology readiness levels (TRL) for these technologies is still low; therefore, there are more opportunities for different processing methods, materials, and products to get in the market. For instance, galvanized by the growing demand for healthcare and Internet-of-Things (IoT) smart devices, the global wearable market size is expected to grow from USD 116.2 billion in 2021 to USD 265.4 billion by 2026 at a growth rate of 18.0% from 2021 to 2026.¹⁷⁰ Along with other printing technologies, LIG

may play a relevant role on the future market of flexible technologies. Therefore, LIG could become fundamental for device fabrication, based on a trade-off between high performance and fast device patterning. Nevertheless, one of the most important advantages of gLIG processing is its sustainable nature and the capability of promoting a greener, circular economy.

In terms of gLIG applicability in electronic component fabrication, this review aimed at showcasing the multifunctionality of this material in a plethora of thin film, in-plane electronic components, and systems. gLIG products present several advantages, such as the ability to pattern complex geometries in a one-step process, while allowing for a simultaneous tuning of surface properties, namely, electrical conductivity, wettability among other aspects such as morphology, giving rise to its multifunctional properties. Furthermore, in-plane components can be readily designed and studied using gLIG, reducing material usage and improving the efficiency when compared to non-planar geometries. However, due to the subtractive, transformative nature of the laser graphitization process, gLIG thin films are eventually restricted and bound to the precursor substrate, slightly restricting their application in thin film technologies where complex layer stacking may be required, a disadvantage when compared to graphene in powder form. Another aspect relevant when developing applications with gLIG is substrate compatibility and durability. Green, bio-based materials have been intensely studied in the electronics field for various purposes, such as transistor fabrication,¹⁷¹ soft and flexible electronics,^{172,173} and even disposable and transient electronics.¹⁷⁴ These efforts ultimately result in pushing several avenues for the advancement of more sustainable fabrication processes, based on circular approaches that promote reusability, recyclability, reducing carbon footprint, and energy consumption in fabrication.¹⁷⁵ As such, the intrinsic properties of natural materials must be carefully selected to meet the requirements of any target application. Both mechanical properties and the ability to be readily converted to gLIG with appropriate characteristics should be taken in consideration, while preserving all the necessary sustainability aspects. Some natural substrates, such as wood and other rigid biomass, are great candidates to be used in rigid application, namely, printed circuit boards.¹⁷⁶ Flexible cellulose or lignin films are attractive for soft, flexible, and wearable technologies. Careful engineering of natural materials’ composition and resulting mechanical and thermal properties is a key aspect for their applicability in specific technologies,¹⁷⁷ also reflecting on gLIG synthesis and applicability. As such, future development on natural composites, using blending and coating approaches are envisioned to improve several aspects of gLIG synthesis, including precursor substrates compatibility and resulting gLIG mechanical, morphological, and conductive properties. In addition, promising work is being presented, regarding the use of new chemical treatments, such as the use of nontoxic, green catalysts, that improve the efficiency and outcome of laser graphitization processes, paired with meticulous control of the laser irradiation process. With the concepts and recent developments discussed in this review and futures work on the synthesis and application of gLIG, challenges related to devices performance, durability, and lifetime may be tackled, while enabling the multi-level integration of different components, using other compatible fabrication technologies such as screen or inkjet printing, to produce hybrid laser engraved and printed systems.

ACKNOWLEDGMENTS

This study was financed in part by Coordenação de Aperfeiçoamento de Pessoal de Nível Superior—Brasil (CAPES)—Finance Code 001. The authors would like to thank the financial support given by CNPq—National Council for Scientific and Technological Development (Grant Nos. 402287/2013–4, 304044/2019–9, and 442575/2019–0), SISNANO/MCTI, Financier of Studies and Projects (FINEP) and Brazilian Agricultural Research Corp. (Embrapa) AgroNano research network. The authors would like to acknowledge the European Commission under the Project NewFun (Grant No. ERC-StG-2014, GA 640598). This work was also supported by European Research Council (ERC) Advanced Grant DIGISMART (Grant No. ERC-AdG-2017, GA 787410) and the FEDER funds through the COMPETE 2020 Program and the National Funds through the FCT—Portuguese Foundation for Science and Technology under the Project No. POCI-01-0145-FEDER-007688, Reference UID/CTM/50025; Project CHIHC, Grant No. PTDC/NAN-MAT/32558/2017; and Project BEST, Grant Nos. ALT20-03-0247-FEDER-113469 and LISBOA-01-0247-FEDER-113469. J. C. acknowledges the Santander/NOVA 2021 Collaborative Research Award—Graphene Smart Bandages for Diabetic Foot Ulcer Monitoring, Reference GSBDFULM. P. C. acknowledges BI-84-Mestre-DIGISMART and CAPES/Embrapa (Grant No. 88882.157024/2017 01) for the scholarships received. S. S. and T. P. also acknowledge the funding from National Foundation for Science and Technology, through the Ph.D. Grant Nos. SFRH/BD/149751/2019 and 2020.08606.BD.

AUTHOR DECLARATIONS

Conflict of Interest

The authors have no conflicts to disclose.

Author Contributions

Pedro Ivo Cunha Claro and Tomás Pinheiro contributed equally to this paper.

Pedro Ivo Cunha Claro: Conceptualization (equal); Writing – original draft (equal); Writing – review & editing (equal). **Tomás Pinheiro:** Conceptualization (equal); Writing – original draft (equal); Writing – review & editing (equal). **Sara L. Silvestre:** Conceptualization (equal); Writing – original draft (equal); Writing – review & editing (equal). **Ana C. Marques:** Conceptualization (equal); Writing – original draft (supporting); Writing – review & editing (supporting). **João Coelho:** Conceptualization (equal); Writing – original draft (supporting); Writing – review & editing (supporting). **José M. Marconcini:** Funding acquisition (equal); Supervision (equal); Writing – review & editing (supporting). **Elvira M. C. Fortunato:** Funding acquisition (equal); Supervision (equal); Writing – review & editing (equal). **Luiz H. C. Mattoso:** Funding acquisition (equal); Supervision (equal); Writing – review & editing (equal). **Rodrigo F. P. Martins:** Funding acquisition (equal); Supervision (equal); Writing – review & editing (equal).

DATA AVAILABILITY

The data that support the findings of this study are available from the corresponding author upon reasonable request.

REFERENCES

- ¹K. S. Novoselov, A. K. Geim, S. V. Morozov, D. Jiang, Y. Zhang, S. V. Dubonos, I. V. Grigorieva, and A. A. Firsov, *Science* **306**, 666 (2004).
- ²R. Ye and J. M. Tour, *ACS Nano* **13**, 10872 (2019).
- ³K. R. Paton, E. Varrla, C. Backes, R. J. Smith, U. Khan, A. O'Neill, C. Boland, M. Lotya, O. M. Istrate, P. King, T. Higgins, S. Barwich, P. May, P. Puczkarski, I. Ahmed, M. Moebius, H. Pettersson, E. Long, J. Coelho, S. E. O'Brien, E. K. McGuire, B. M. Sanchez, G. S. Duesberg, N. McEvoy, T. J. Pennycook, C. Downing, A. Crossley, V. Nicolosi, and J. N. Coleman, *Nat. Mater.* **13**, 624 (2014).
- ⁴A. J. Mannix, B. Kiraly, M. C. Hersam, and N. P. Guisinger, *Nat. Rev. Chem.* **1**, 0014 (2017).
- ⁵Sigma-Aldrich, Graphene ink for inkjet printing, 2022.
- ⁶Sigma-Aldrich, Molybdenum disulfide ink for spin/spray coating, 2022.
- ⁷S. P. Singh, Y. Li, A. Be'er, Y. Oren, J. M. Tour, and C. J. Arnsch, *ACS Appl. Mater. Interfaces* **9**, 18238 (2017).
- ⁸F. Wang, K. Wang, B. Zheng, X. Mei, J. Lv, W. Duan, and W. Wang, *Mater. Technol.* **33**, 340 (2018).
- ⁹F. M. Vivaldi, A. Dallinger, A. Bonini, N. Poma, L. Sembranti, D. Biagini, P. Salvo, F. Greco, and F. D. Francesco, *ACS Appl. Mater. Interfaces* **13**, 30245 (2021).
- ¹⁰R. Ye, Z. Peng, T. Wang, Y. Xu, J. Zhang, Y. Li, L. G. Nilewski, J. Lin, and J. M. Tour, *ACS Nano* **9**, 9244 (2015).
- ¹¹J. Zhu, D. Yang, Z. Yin, Q. Yan, and H. Zhang, *Small* **10**, 3480 (2014).
- ¹²A. G. Olabi, M. A. Abdelkareem, T. Wilberforce, and E. T. Sayed, *Renewable Sustainable Energy Rev.* **135**, 110026 (2021).
- ¹³A. Nag, A. Mitra, and S. C. Mukhopadhyay, *Sens. Actuators, A* **270**, 177 (2018).
- ¹⁴S.-H. Bae, Y. Lee, B. K. Sharma, H.-J. Lee, J.-H. Kim, and J.-H. Ahn, *Carbon* **51**, 236 (2013).
- ¹⁵K. Yam, N. Guo, Z. Jiang, S. Li, and C. Zhang, *Catalysts* **10**, 53 (2020).
- ¹⁶Z. Niu, L. Liu, L. Zhang, and X. Chen, *Small* **10**, 3434 (2014).
- ¹⁷K. Pal, A. Si, G. S. El-Sayyad, M. A. Elkindous, R. Kumar, A. I. El-Batal, S. Kralj, and S. Thomas, *Crit. Rev. Solid State Mater. Sci.* **46**, 385 (2021).
- ¹⁸R. Ye, D. K. James, and J. M. Tour, *Acc. Chem. Res.* **51**, 1609 (2018).
- ¹⁹H. Huang, H. Shi, P. Das, J. Qin, Y. Li, X. Wang, F. Su, P. Wen, S. Li, P. Lu, F. Liu, Y. Li, Y. Zhang, Y. Wang, Z. Wu, and H. Cheng, *Adv. Funct. Mater.* **30**, 1909035 (2020).
- ²⁰V. Strauss, K. Marsh, M. D. Kowal, M. El-Kady, and R. B. Kaner, *Adv. Mater.* **30**, 1704449 (2018).
- ²¹Y. Tao, Z.-Y. Sui, and B.-H. Han, *J. Mater. Chem. A* **8**, 6125 (2020).
- ²²Z. Wan, N.-T. Nguyen, Y. Gao, and Q. Li, *Sustainable Mater. Technol.* **25**, e00205 (2020).
- ²³B. Huet, J.-P. Raskin, D. W. Snyder, and J. M. Redwing, *Carbon* **163**, 95 (2020).
- ²⁴Y. Xu, H. Cao, Y. Xue, B. Li, and W. Cai, *Nanomaterials* **8**, 942 (2018).
- ²⁵R. Ye, D. K. James, and J. M. Tour, *Adv. Mater.* **31**, 1803621 (2019).
- ²⁶M. F. El-Kady, V. Strong, S. Dubin, and R. B. Kaner, *Science* **335**, 1326 (2012).
- ²⁷R. Mukherjee, A. V. Thomas, A. Krishnamurthy, and N. Koratkar, *ACS Nano* **6**, 7867 (2012).
- ²⁸J. Lin, Z. Peng, Y. Liu, F. Ruiz-Zepeda, R. Ye, E. L. G. Samuel, M. J. Yacaman, B. I. Yakobson, and J. M. Tour, *Nat. Commun.* **5**, 5714 (2014).
- ²⁹V. N. Ataide, W. A. Ameku, R. P. Bacil, L. Angnes, W. R. De Araujo, and T. Paixão, *RSC Adv.* **11**, 1644 (2021).
- ³⁰N. C. Y. Tham, P. K. Sahoo, Y. Kim, C. Hegde, S. W. Lee, Y. Kim, and V. M. Murukeshan, *Adv. Mater. Technol.* **6**, 2001156 (2021).
- ³¹P. I. C. Claro, A. C. Marques, I. Cunha, R. F. P. Martins, L. M. N. Pereira, J. M. Marconcini, L. H. C. Mattoso, and E. Fortunato, *ACS Appl. Nano Mater.* **4**, 8262 (2021).
- ³²S. Lee and S. Jeon, *ACS Sustainable Chem. Eng.* **7**, 2270 (2019).
- ³³J. Edberg, R. Brooke, O. Hosseinaei, A. Fall, K. Wijeratne, and M. Sandberg, *npj Flexible Electron.* **4**, 17 (2020).
- ³⁴C. Zhang, Y. Xie, C. Zhang, and J. Lin, *Carbon* **153**, 585 (2019).
- ³⁵S. Lee, H. Jang, H. Lee, D. Yoon, and S. Jeon, *ACS Appl. Mater. Interfaces* **11**, 26970 (2019).

- ³⁶M. G. Stanford, J. T. Li, Y. Chyan, Z. Wang, W. Wang, and J. M. Tour, *ACS Nano* **13**, 7166 (2019).
- ³⁷X. Zang, C. Shen, Y. Chu, B. Li, M. Wei, J. Zhong, M. Sanghadasa, and L. Lin, *Adv. Mater.* **30**, 1800062 (2018).
- ³⁸T. D. Le, S. Park, J. An, P. S. Lee, and Y. Kim, *Adv. Funct. Mater.* **29**, 1902771 (2019).
- ³⁹P. Yadav, A. Basu, A. Suryawanshi, O. Game, and S. Ogale, *Adv. Mater. Interfaces* **3**, 1600057 (2016).
- ⁴⁰Z. Peng, R. Ye, J. A. Mann, D. Zakhidov, Y. Li, P. R. Smalley, J. Lin, and J. M. Tour, *ACS Nano* **9**, 5868 (2015).
- ⁴¹T. D. Le, Y. A. Lee, H. K. Nam, K. Y. Jang, D. Yang, B. Kim, K. Yim, S. Kim, H. Yoon, and Y. Kim, *Adv. Funct. Mater.* **32**, 2107768 (2022).
- ⁴²Y. Chyan, R. Ye, Y. Li, S. P. Singh, C. J. Arnusch, and J. M. Tour, *ACS Nano* **12**, 2176 (2018).
- ⁴³R. Ye, Y. Chyan, J. Zhang, Y. Li, X. Han, C. Kittrell, and J. M. Tour, *Adv. Mater.* **29**, 1702211 (2017).
- ⁴⁴W. R. de Araujo, C. M. R. Frasson, W. A. Ameku, J. R. Silva, L. Angnes, and T. Paixão, *Angew. Chem.* **129**, 15309 (2017).
- ⁴⁵T. Pinheiro, S. Silvestre, J. Coelho, A. C. Marques, R. Martins, M. G. F. Sales, and E. Fortunato, *Adv. Mater. Interfaces* **8**, 2101502 (2021).
- ⁴⁶A. Imbrogno, J. Islam, C. Santillo, R. Castaldo, L. Sygellou, C. Larrigy, R. Murray, E. Vaughan, M. K. Hoque, A. J. Quinn, and D. Iacopino, *ACS Appl. Electron. Mater.* **4**, 1541 (2022).
- ⁴⁷B. Kulyk, M. Matos, B. F. R. Silva, A. F. Carvalho, A. J. S. Fernandes, D. V. Evtuguin, E. Fortunato, and F. M. Costa, *Diamond Relat. Mater.* **123**, 108855 (2022).
- ⁴⁸F. Mahmood, Y. Sun, and C. Wan, *RSC Adv.* **11**, 15410 (2021).
- ⁴⁹B. Kulyk, B. F. R. Silva, A. F. Carvalho, S. Silvestre, A. J. S. Fernandes, R. Martins, E. Fortunato, and F. M. Costa, *ACS Appl. Mater. Interfaces* **13**, 10210 (2021).
- ⁵⁰P. Zhao, G. Bhattacharya, S. J. Fishlock, J. G. M. Guy, A. Kumar, C. Tsonos, Z. Yu, S. Raj, J. A. McLaughlin, J. Luo, and N. Soin, *Nano Energy* **75**, 104958 (2020).
- ⁵¹X. Sun, X. Liu, and F. Li, *Appl. Surf. Sci.* **551**, 149438 (2021).
- ⁵²S. Nandy, S. Goswami, A. Marques, D. Gaspar, P. Grey, I. Cunha, D. Nunes, A. Pimentel, R. Igreja, P. Barquinha, L. Pereira, E. Fortunato, and R. Martins, *Adv. Mater. Technol.* **6**, 2000994 (2021).
- ⁵³M. Terakawa, *Handbook of Laser Micro-Nano-Engineering* (Springer International Publishing, Cham, 2021), pp. 1–22.
- ⁵⁴N. Bituyurin, B. S. Luk'yanchuk, M. H. Hong, and T. C. Chong, *Chem. Rev.* **103**, 519 (2003).
- ⁵⁵S. Chatani, C. J. Kloxin, and C. N. Bowman, *Polym. Chem.* **5**, 2187 (2014).
- ⁵⁶N. Arnold, N. Bituyurin, and D. Bäuerle, *Appl. Surf. Sci.* **138–139**, 212 (1999).
- ⁵⁷A. Cogulet, P. Blanchet, and V. Landry, *J. Photochem. Photobiol., B* **158**, 184 (2016).
- ⁵⁸T. Kawasaki, H. Zen, T. Sakai, Y. Sumitomo, K. Nogami, K. Hayakawa, T. Yaji, T. Ohta, T. Nagata, and Y. Hayakawa, *Polymers* **14**, 2401 (2022).
- ⁵⁹T. Kawasaki, T. Sakai, H. Zen, Y. Sumitomo, K. Nogami, K. Hayakawa, T. Yaji, T. Ohta, K. Tsukiyama, and Y. Hayakawa, *Energy Fuels* **34**, 9064 (2020).
- ⁶⁰T. D. Le, H. Phan, S. Kwon, S. Park, Y. Jung, J. Min, B. J. Chun, H. Yoon, S. H. Ko, S. Kim, and Y. Kim, *Adv. Funct. Mater.* **2205158** (2022).
- ⁶¹M. Devi, S. Rawat, and S. Sharma, *Oxford Open Mater. Sci.* **1**, itab014 (2020).
- ⁶²M. G. Stanford, C. Zhang, J. D. Fowlkes, A. Hoffman, I. N. Ivanov, P. D. Rack, and J. M. Tour, *ACS Appl. Mater. Interfaces* **12**, 10902 (2020).
- ⁶³I. R. Hristovski, L. A. Herman, M. E. Mitchell, N. I. Lesack, J. Reich, and J. F. Holzman, *Nanomaterials* **12**, 1241 (2022).
- ⁶⁴J. Kolar, M. Strlic, S. Pentzien, and W. Kautek, *Appl. Phys. A* **71**, 87 (2000).
- ⁶⁵L. Wang, Z. Wang, A. N. Bakhtiyari, and H. Zheng, *Micromachines* **11**, 1094 (2020).
- ⁶⁶G. Li, *J. Appl. Phys.* **127**, 010901 (2020).
- ⁶⁷H. Park, M. Kim, B. G. Kim, and Y. H. Kim, *ACS Appl. Nano Mater.* **3**, 6899 (2020).
- ⁶⁸S. Lee, J. Eun, and S. Jeon, *Nano Energy* **68**, 104364 (2020).
- ⁶⁹A. M. Dimiev, G. Ceriotti, N. Behabtu, D. Zakhidov, M. Pasquali, R. Saito, and J. M. Tour, *ACS Nano* **7**, 2773 (2013).
- ⁷⁰F. Morosawa, S. Hayashi, M. Terakawa, and A. C. S. Sustain, *Chem. Eng.* **9**, 2955 (2021).
- ⁷¹Y. Li, D. X. Luong, J. Zhang, Y. R. Tarkunde, C. Kittrell, F. Sargunraj, Y. Ji, C. J. Arnusch, and J. M. Tour, *Adv. Mater.* **29**, 1700496 (2017).
- ⁷²E. R. Mamleyev, S. Heissler, A. Nefedov, P. G. Weidler, N. Nordin, V. V. Kudryashov, K. Länge, N. MacKinnon, and S. Sharma, *npj Flexible Electron* **3**(2), 1 (2019).
- ⁷³Q. Meng, J. Yan, R. Wu, H. Liu, Y. Sun, N. Wu, J. Xiang, L. Zheng, J. Zhang, and B. Han, *Nat. Commun.* **12**, 4534 (2021).
- ⁷⁴A. Vashisth, M. Kowalik, J. C. Geringer, C. Ashraf, A. C. T. van Duin, and M. J. Green, *ACS Appl. Nano Mater.* **3**, 1881 (2020).
- ⁷⁵H. Kawamoto, *J. Wood Sci.* **63**, 117 (2017).
- ⁷⁶M. Alhrech, S. Omolabake, C. M. Holland, G. E. Klinger, E. L. Hegg, and S. S. Stahl, *ACS Cent. Sci.* **7**, 1831 (2021).
- ⁷⁷H. Zhou, C. Wu, J. A. Onwudili, A. Meng, Y. Zhang, and P. T. Williams, *Energy Fuels* **28**, 6371 (2014).
- ⁷⁸X.-Y. Wang, X. Yao, and K. Müllen, *Sci. China Chem.* **62**, 1099 (2019).
- ⁷⁹D. B. Wiedemeier, S. Abiven, W. C. Hockaday, M. Keiluweit, M. Kleber, C. A. Masiello, A. V. McBeath, P. S. Nico, L. A. Pyle, M. P. W. Schneider, R. J. Smernik, G. L. B. Wiesenberger, and M. W. I. Schmidt, *Org. Geochem.* **78**, 135 (2015).
- ⁸⁰X. Zang, C. Jian, S. Ingersoll, H. Li, J. J. Adams, Z. Lu, N. Ferralis, and J. C. Grossman, *Sci. Adv.* **6**, 1 (2020).
- ⁸¹X. Zang, N. Ferralis, and J. C. Grossman, *ACS Nano* **16**, 2101 (2022).
- ⁸²M. Wohler, T. Benselfelt, L. Wågberg, I. Furró, L. A. Berglund, and J. Wohler, *Cellulose* **29**, 1 (2022).
- ⁸³P. Bajpai, *Biermann's Handbook of Pulp and Paper* (Elsevier, 2018), pp. 19–74.
- ⁸⁴Y. Yao, X. Duan, M. Niu, J. Luo, R. Wang, and T. Liu, *Cellulose* **26**, 7423 (2019).
- ⁸⁵M. J. Nine, D. N. H. Tran, T. T. Tung, S. Kabiri, and D. Losic, *ACS Appl. Mater. Interfaces* **9**, 10160 (2017).
- ⁸⁶Z. A. Nagieb, M. A. Nassar, and M. G. El-Meligy, *Int. J. Carbohydr. Chem.* **2011**, 146763.
- ⁸⁷Y. Chyan, J. Cohen, W. Wang, C. Zhang, and J. M. Tour, *ACS Appl. Nano Mater.* **2**, 3007 (2019).
- ⁸⁸K. M. Clark, L. Skrajewski, T. E. Benavidez, L. F. Mendes, E. L. Bastos, F. A. Dörr, R. Sachdeva, A. A. Ogale, T. Paixão, and C. D. Garcia, *Soft Matter* **16**, 7659 (2020).
- ⁸⁹S. Xin, H. Yang, Y. Chen, M. Yang, L. Chen, X. Wang, and H. Chen, *J. Anal. Appl. Pyrolysis* **116**, 263 (2015).
- ⁹⁰X. Zhou, W. Li, R. Mabon, and L. J. Broadbelt, *Energy Technol.* **5**, 52 (2017).
- ⁹¹F. Cheng and X. Li, *Catalysts* **8**, 346 (2018).
- ⁹²T. E. McGrath, W. G. Chan, and M. R. Hajaligol, *J. Anal. Appl. Pyrolysis* **66**, 51 (2003).
- ⁹³Y. Yang, Z. Luo, S. Li, K. Lu, and W. Wang, *BioResources* **14**, 5816 (2019).
- ⁹⁴J. Hidalgo-Carrillo, A. Marinas, and F. J. Urbano, in *Furfural: An Entry Point Lignocellulose in Biorefineries to Produce Renewable Chemicals, Polymers, and Biofuels* (World Scientific Publishing Company, 2018), pp. 1–30.
- ⁹⁵H. Yang, M. Gong, J. Hu, B. Liu, Y. Chen, J. Xiao, S. Li, Z. Dong, and H. Chen, *Energy Fuels* **34**, 3412 (2020).
- ⁹⁶B. Zhang, J. Song, G. Yang, and B. Han, *Chem. Sci.* **5**, 4656 (2014).
- ⁹⁷A. Reina, X. Jia, J. Ho, D. Nezhich, H. Son, V. Bulovic, M. S. Dresselhaus, and J. Kong, *Nano Lett.* **9**, 30 (2008).
- ⁹⁸S. Y. Jeong, C. W. Lee, J. U. Lee, Y. W. Ma, and B. S. Shin, *Nanomaterials* **10**, 1904 (2020).
- ⁹⁹W. Qu, Z. Zhao, J. Wang, F. Dong, H. Xu, X. Sun, and H. Jin, *Sustainable Energy Fuels* **5**, 3744 (2021).
- ¹⁰⁰V. Scardaci and G. Compagnini, *J. Carbon Res.* **7**, 48 (2021).
- ¹⁰¹B. Kulyk, B. F. R. Silva, A. F. Carvalho, P. Barbosa, A. V. Girão, J. Deuermeier, A. J. S. Fernandes, F. M. L. Figueiredo, E. Fortunato, and F. M. Costa, *Adv. Mater. Technol.* **7**, 2101311 (2022).
- ¹⁰²F. Mahmood, C. Zhang, Y. Xie, D. Stalla, J. Lin, and C. Wan, *RSC Adv.* **9**, 22713 (2019).
- ¹⁰³S. Wang, Y. Yu, S. Luo, X. Cheng, G. Feng, Y. Zhang, Z. Wu, G. Compagnini, J. Pooran, and A. Hu, *Appl. Phys. Lett.* **115**, 083904 (2019).
- ¹⁰⁴H. Estrade-Szwarckopf, *Carbon* **42**, 1713 (2004).
- ¹⁰⁵L. F. Mendes, A. de Siervo, W. Reis de Araujo, and T. R. Longo Cesar Paixão, *Carbon* **159**, 110 (2020).

- ¹⁰⁶X. Han, R. Ye, Y. Chyan, T. Wang, C. Zhang, L. Shi, T. Zhang, Y. Zhao, and J. M. Tour, *ACS Appl. Nano Mater.* **1**, 5053 (2018).
- ¹⁰⁷N. Tasić, A. Bezerra Martins, X. Yifei, M. Sousa Góes, D. Martín-Yerga, L. Mao, T. Paixão, and L. Moreira Gonçalves, *Electrochem. Commun.* **121**, 106872 (2020).
- ¹⁰⁸K. Sinha, L. Meng, Q. Xu, and X. Wang, *Mater. Lett.* **286**, 129268 (2021).
- ¹⁰⁹D. B. Schuepfer, F. Badaczewski, J. M. Guerra-Castro, D. M. Hofmann, C. Heiliger, B. Smarsly, and P. J. Klar, *Carbon* **161**, 359 (2020).
- ¹¹⁰C. H. Dreimol, H. Guo, M. Ritter, T. Keplinger, Y. Ding, R. Günther, E. Poloni, I. Burgert, and G. Panzarasa, *Nat. Commun.* **13**, 3680 (2022).
- ¹¹¹L. G. Cançado, A. Jorio, E. H. M. Ferreira, F. Stavale, C. A. Achete, R. B. Capaz, M. V. O. Moutinho, A. Lombardo, T. S. Kulmala, and A. C. Ferrari, *Nano Lett.* **11**, 3190 (2011).
- ¹¹²Y. Zhu, S. Murali, M. D. Stoller, K. J. Ganesh, W. Cai, P. J. Ferreira, A. Pirkle, R. M. Wallace, K. A. Cychosz, M. Thommes, D. Su, E. A. Stach, and R. S. Ruoff, *Science* **332**, 1537 (2011).
- ¹¹³C. Su, M. Acik, K. Takai, J. Lu, S. J. Hao, Y. Zheng, P. Wu, Q. Bao, T. Enoki, Y. J. Chabal, and K. P. Loh, *Nat. Commun.* **3**, 1298 (2012).
- ¹¹⁴J. Ma, D. Alfé, A. Michaelides, and E. Wang, *Phys. Rev. B* **80**, 033407 (2009).
- ¹¹⁵A. Kumar, T. Jyske, and M. Petrič, *Adv. Sustainable Syst.* **5**, 2000251 (2021).
- ¹¹⁶M. Mariana, T. Alfatah, A. K. H.P.S, E. B. Yahya, N. G. Olaiya, A. Nuryawan, E. M. Mistar, C. K. Abdullah, S. N. Abdulmajid, and H. Ismail, *J. Mater. Res. Technol.* **15**, 2287 (2021).
- ¹¹⁷A. R. Sena Neto, M. A. M. Araujo, R. M. P. Barboza, A. S. Fonseca, G. H. D. Tonoli, F. V. Souza, L. H. C. Mattoso, and J. M. Marconcini, *Ind. Crops Prod.* **64**, 68 (2015).
- ¹¹⁸A. Garcia-Maraver, D. Salvachúa, M. J. Martínez, L. F. Diaz, and M. Zamorano, *Waste Manag.* **33**, 2245 (2013).
- ¹¹⁹A. P. Duarte and J. C. Bordado, *Front. Mater.* **2**, 2 (2015).
- ¹²⁰S. R. Karade, F. Caldiera, M. Irle, and K. Maher, in *Challenges of Concrete Construction: Vol. 5. Sustainable Concrete Construction* (Thomas Telford Publishing, 2002), pp. 253–261.
- ¹²¹A. Costa, I. Barbosa, C. Miguel, and J. Graça, *Ann. Sci.* **78**, 52 (2021).
- ¹²²M. A. A. Ahamed, M. S. A. Perera, S. K. Matthai, P. G. Ranjith, and L. Dongyin, *J. Pet. Sci. Eng.* **180**, 901 (2019).
- ¹²³H. Jang, J. Choi, H. Lee, and S. Jeon, *ACS Appl. Mater. Interfaces* **12**, 30320 (2020).
- ¹²⁴A. F. Carvalho, A. J. S. Fernandes, R. Martins, E. Fortunato, and F. M. Costa, *Adv. Mater. Technol.* **5**, 2000630 (2020).
- ¹²⁵L. Dessbesell, M. Paleologou, M. Leitch, R. Pulkki, and C. (Charles) Xu, *Renewable Sustainable Energy Rev.* **123**, 109768 (2020).
- ¹²⁶S. Zeng, J. Zhang, G. Zu, and J. Huang, *Carbohydr. Polym.* **267**, 118198 (2021).
- ¹²⁷S. Agate, M. Joyce, L. Lucia, and L. Pal, *Carbohydr. Polym.* **198**, 249 (2018).
- ¹²⁸M. Li, Z. Bi, L. Xie, G. Sun, Z. Liu, Q. Kong, X. Wei, and C. M. Chen, *ACS Sustainable Chem. Eng.* **7**, 14796 (2019).
- ¹²⁹L. Zhu, Y. Huang, Y. Morishita, K. Uetani, M. Nogi, and H. Koga, *J. Mater. Chem. C* **9**, 4444 (2021).
- ¹³⁰V. K. Thakur, M. K. Thakur, P. Raghavan, M. R. Kessler, and A. C. S. Sustain, *Chem. Eng.* **2**, 1072 (2014).
- ¹³¹X. Sun, H. Jin, and W. Qu, *RSC Adv.* **11**, 19695 (2021).
- ¹³²W. Zhang, Y. Lei, F. Ming, Q. Jiang, P. Costa, and H. N. Alshareef, *Adv. Energy Mater.* **8**, 1801840 (2018).
- ¹³³Y. Lei, W. Zhao, Y. Zhu, U. Buttner, X. Dong, and H. N. Alshareef, *ACS Nano* **16**, 1974 (2022).
- ¹³⁴Y. Lei, A. H. Alshareef, W. Zhao, and S. Inal, *ACS Appl. Nano Mater.* **3**, 1166 (2020).
- ¹³⁵E. Fortunato, N. Correia, P. Barquinha, L. Pereira, G. Goncalves, and R. Martins, *IEEE Electron Device Lett.* **29**, 988 (2008).
- ¹³⁶L. Pereira, D. Gaspar, D. Guerin, A. Delattre, E. Fortunato, and R. Martins, *Nanotechnology* **25**, 094007 (2014).
- ¹³⁷R. Martins, P. Barquinha, L. Pereira, N. Correia, G. Gonçalves, I. Ferreira, and E. Fortunato, *Appl. Phys. Lett.* **93**, 203501 (2008).
- ¹³⁸I. Ferreira, B. Brás, N. Correia, P. Barquinha, E. Fortunato, and R. Martins, *J. Disp. Technol.* **6**, 332 (2010).
- ¹³⁹A. Nathan, N. Correia, R. Barros, R. Martins, R. Costa, L. Pereira, I. Ferreira, A. Ahnood, E. Fortunato, and P. Barquinha, *Adv. Mater.* **23**, 4491 (2011).
- ¹⁴⁰D. Gaspar, J. Martins, P. Bahubalindruni, L. Pereira, E. Fortunato, and R. Martins, *Adv. Electron. Mater.* **4**, 1800423 (2018).
- ¹⁴¹S. M. Khan, J. M. Nassar, and M. M. Hussain, *ACS Appl. Electron. Mater.* **3**, 30 (2021).
- ¹⁴²P. Bajpai, *Green Chemistry and Sustainability in Pulp and Paper Industry* (Springer International Publishing, Cham, 2015).
- ¹⁴³J. Shen, Z. Song, X. Qian, and Y. Ni, *Ind. Eng. Chem. Res.* **50**, 661 (2011).
- ¹⁴⁴K. Niskanen, *Mechanics of Paper Products* (Walter de Gruyter, 2011).
- ¹⁴⁵P. Grey, S. N. Fernandes, D. Gaspar, J. Deurmeier, R. Martins, E. Fortunato, M. H. Godinho, and L. Pereira, *ACS Appl. Electron. Mater.* **2**, 426 (2020).
- ¹⁴⁶D. Gaspar, S. N. Fernandes, A. G. de Oliveira, J. G. Fernandes, P. Grey, R. V. Pontes, L. Pereira, R. Martins, M. H. Godinho, and E. Fortunato, *Nanotechnology* **25**, 094008 (2014).
- ¹⁴⁷M. Nogi, S. Iwamoto, A. N. Nakagaito, and H. Yano, *Adv. Mater.* **21**, 1595 (2009).
- ¹⁴⁸V. Thakur, A. Guleria, S. Kumar, S. Sharma, and K. Singh, *Mater. Adv.* **2**, 1872 (2021).
- ¹⁴⁹N. Tasić, L. Sousa de Oliveira, T. Paixão, and L. Moreira Gonçalves, *Med. Devices Sens.* **3**, e10115 (2020).
- ¹⁵⁰K. Ju, Y. Gao, T. Xiao, C. Yu, J. Tan, and F. Xuan, *RSC Adv.* **10**, 18694 (2020).
- ¹⁵¹A. Kothuru, C. H. Rao, and S. Goel, in *2021 IEEE International Flexible Electronics Technology Conference (IEEE, 2021)*, pp. 0050–0052.
- ¹⁵²M. Reynolds, L. M. Duarte, W. K. T. Coltro, M. F. Silva, F. J. V. Gomez, and C. D. Garcia, *Microchem. J.* **157**, 105067 (2020).
- ¹⁵³B. Kulyk, S. O. Pereira, A. J. S. Fernandes, E. Fortunato, F. M. Costa, and N. F. Santos, *Carbon* **197**, 253 (2022).
- ¹⁵⁴G. Bhattacharya, S. J. Fishlock, S. Hussain, S. Choudhury, A. Xiang, B. Kandola, A. Pritam, N. Soim, S. S. Roy, and J. A. McLaughlin, *ACS Appl. Mater. Interfaces* **14**, 31109 (2022).
- ¹⁵⁵Y. Jung, J. Min, J. Choi, J. Bang, S. Jeong, K. R. Pyun, J. Ahn, Y. Cho, S. Hong, S. Hong, J. Lee, and S. H. Ko, *Appl. Mater. Today* **29**, 101589 (2022).
- ¹⁵⁶N. Kumar, R. Salehiyan, V. Chauke, O. J. Bothoko, K. Setshedi, M. Scriba, M. Masukume, and S. Sinha Ray, *FlatChem* **27**, 100224 (2021).
- ¹⁵⁷A. S. Sharova, F. Melloni, G. Lanzani, C. J. Bettinger, and M. Caironi, *Adv. Mater. Technol.* **6**, 2000757 (2021).
- ¹⁵⁸M. Athanasiou, N. Samartzis, L. Sygellou, V. Dracopoulos, T. Ioannides, and S. N. Yannopoulos, *Carbon* **172**, 750 (2021).
- ¹⁵⁹S. Delacroix, H. Wang, T. Heil, and V. Strauss, *Adv. Electron. Mater.* **6**, 2000463 (2020).
- ¹⁶⁰Y. Lin, Q. Zhang, Y. Deng, K. Shen, K. Xu, Y. Yu, S. Wang, and G. Fang, *ACS Sustainable Chem. Eng.* **9**, 3112 (2021).
- ¹⁶¹G. F. Hawes, D. Yilmaz, B. S. Noremberg, and M. A. Pope, *ACS Appl. Nano Mater.* **2**, 6312 (2019).
- ¹⁶²Y.-H. Huang, S.-J. Ni, and L. Li, *Lasers Eng.* **46**, 321 (2020).
- ¹⁶³C. Zhou, K. Zhang, M. Hong, Y. Yang, N. Hu, Y. Su, L. Zhang, and Y. Zhang, *Chem. Eng. J.* **385**, 123720 (2020).
- ¹⁶⁴V. Scardaci, *Appl. Sci.* **11**, 6304 (2021).
- ¹⁶⁵X. Wu, F. Mu, and Z. Lin, *Mater. Today Adv.* **11**, 100157 (2021).
- ¹⁶⁶L. Cheng, W. Guo, X. Cao, Y. Dou, L. Huang, Y. Song, J. Su, Z. Zeng, and R. Ye, *Mater. Chem. Front.* **5**, 4874 (2021).
- ¹⁶⁷F. Catania, E. Marras, M. Giorcelli, P. Jagdale, L. Lavagna, A. Tagliaferro, and M. Bartoli, *Appl. Sci.* **11**, 614 (2021).
- ¹⁶⁸S. Pinilla, J. Coelho, K. Li, J. Liu, and V. Nicolosi, *Nat. Rev. Mater.* **7**, 717 (2022).
- ¹⁶⁹M. A. M. Leenen, V. Arning, H. Thiem, J. Steiger, and R. Anselmann, *Phys. Status Solidi* **206**, 588 (2009).
- ¹⁷⁰Markets and Markets Research Ltd., Market Research Report No. SE2763, 2021.
- ¹⁷¹F. Torricelli, I. Alessandri, E. Macchia, I. Vassalini, M. Maddaloni, and L. Torsi, *Adv. Mater. Technol.* **7**, 2100445 (2022).
- ¹⁷²D. Gao, J. Lv, and P. S. Lee, *Adv. Mater.* **34**, 2105020 (2022).
- ¹⁷³L. Lan, J. Ping, J. Xiong, and Y. Ying, *Adv. Sci.* **9**, 2200560 (2022).
- ¹⁷⁴A. O. Chinomso Iroegbu and S. S. Ray, *ACS Omega* **7**, 10854 (2022).
- ¹⁷⁵N. A. Tarazona, R. Machatschek, J. Balcucho, J. L. Castro-Mayorga, J. F. Saldarriaga, and A. Lendlein, *MRS Energy Sustainability* **9**, 28 (2022).
- ¹⁷⁶K. Immonen, J. Lyytikäinen, J. Keränen, K. Eiroma, M. Suhonen, M. Vikman, V. Leminen, M. Välimäki, and L. Hakola, *Materials* **15**, 2679 (2022).
- ¹⁷⁷H. Zhu, W. Luo, P. N. Ciesielski, Z. Fang, J. Y. Zhu, G. Henriksson, M. E. Himmel, and L. Hu, *Chem. Rev.* **116**, 9305 (2016).